ACS OMEGA

Open Access

This article is licensed under CC-BY-NC-ND 4.0

http://pubs.acs.org/journal/acsodf

Article

An Exploratory Experimental Analysis Backed by Quantum Mechanical Modeling, Spectroscopic, and Surface Study for C-Steel Surface in the Presence of Hydrazone-Based Schiff Bases to Fix Corrosion Defects in Acidic Media

Amira H. E. Moustafa,* Hanaa H. Abdel-Rahman, Assem Barakat, Hagar A. Mohamed, and Ahmed S. El-Kholany

Cite This: *ACS Omega* 2024, 9, 16469−16485

Read Online

ACCESS | Metrics & More | Article Recommendations | Supporting Information

ABSTRACT: This work focuses on developing corrosion control and protecting the environment by creating affordable, sustainable, environmentally friendly, and efficient corrosion resistance chemicals. That is, through synthesized three hydrazone Schiff bases *E*-2-(1-hydrazonoethyl)-thiazole (**HTZ**), 2-((*E*)-(((*Z*)-1-(thiazol-2-yl)ethylidene)hydrazono)-methyl)phenol (**HTZS**), and 2-((*E*)-(((*Z*)-1-(pyridin-2-yl)ethylidene)-hydrazono)methyl)phenol (**HPYS**) and corrosion inhibitors for C-steel in 8 M H_3PO_4 solution that were studied. The chemicals were analyzed by using ^1H NMR and ^{13}C NMR spectroscopy to learn more about them. Predominantly, the hydrazone-based Schiff bases have been considered powerful inhibitors due to their ability to be adsorbed with very low concentrations through their reactive sites (N, O, and S). Maximum surface (θ_{max}) coverage and inhibition efficiency of 83.33% were sufficiently found at 99.00×10^{-3} mol/L concentration of **HTZS** at 293 K. Galvanostatic experiments demonstrated that raising the concentration of hydrazones improved mass transfer resistance. To study microstructure, scanning, reflectance, and energy-dispersive X-rays were used. Roughness and qualitative adhesion of the adsorbed layer were estimated by an atomic force microscope. After adding 99.00×10^{-3} mol/L of **HTZS**, the degree of surface brightness and reflectance increases to 137.20, relative to the corroded electrolyte-free solution 27.70. The roughness (Ra) decreased from 0.468 to 0.088 μm by adding **HTZS**. A surface morphology study confirmed that adding hydrazones to the C-steel dissolution bath greatly improves the surface's look and texture quality. The atomic absorption spectroscopy technique was used to compare the concentration of the iron ions that remained in the solution after galvanostatic analysis in the absence and presence of the hydrazones under different conditions; it was found that the inhibited solution contained lower concentrations of iron ions as compared to the uninhibited solution. The DFT theoretical analysis verified the observation of hydrazone physical adsorption through bonding electrons that obey kinetic adsorption isotherms. It is based on examining the highest occupied molecular orbital−lowest occupied molecular orbital (HOMO−LUMO), the Fukui functions, and the Mulliken atomic charge. Overall, the results suggest that **HTZS** is a good corrosion inhibitor with a large surface area due to the presence of S, N, and O atoms, allowing for creating a larger surface due to the large molecular volume of atoms protecting against the corrosion process.

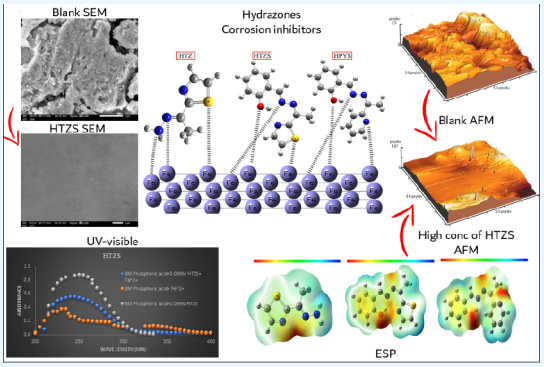

INTRODUCTION

Metal is a vital raw material that has fostered industrial growth and played a crucial part in the development of human civilization. Industrial metals frequently experience corrosion, which has a negative influence on both their cost and safety. The use of metals that resist corrosion better is a wise decision. Cost-effective and commonly used ways to avoid metal corrosion include optimizing the metal's components and smelting process, using organic/inorganic coating technology, and adding corrosion inhibitors.[1,2]

Carbon steel (C-steel) is a common metal utilized in the industry since it is thought to be more efficient and cost-effective. The research on carbon steel's corrosion inhibition behavior is the most popular in literature surveys, partly because carbon steel has relatively high strength, is inexpensive, and is widely used in many industrial fields. Carbon steel, on the other hand, corrodes easily. Iron is a highly reactive

Received: January 6, 2024
Revised: March 8, 2024
Accepted: March 12, 2024
Published: March 28, 2024

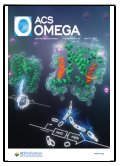

© 2024 The Authors. Published by American Chemical Society

material; therefore, corrosion occurs often throughout its manufacture and usage. This is especially true in the chemical and petrochemical industries; robust acidic solutions come into direct contact with carbon steel, shortening their service life and potentially increasing the risk of major accidents.[3,4]

In many industrial operations, scale and rust are typically removed with acid solutions. Phosphoric acid (H_3PO_4) is a significant industrial chemical used as an intermediary in the fertilizer industry for metal surface treatment in the metallurgical sector because it is less corrosive than other mineral acids. It is employed in passivating, phosphating, chemical coloring, oxide coating removal, chemical and electrolytic polishing or etching, and surface cleaning. It exhibits considerable corrosiveness on C-steel despite its relevance. Accordingly, the C-steel corrosion in phosphoric acid was slowed down or prevented by adding anticorrosion agents. In these procedures, inhibitors are utilized to regulate both the amount of acid consumed and the dissolution of metals.[5,6]

Any inhibitor's performance can be determined by testing how well it prevents C-steel corrosion under acidic conditions. It is assumed that industrial research is currently of interest in this area. Schiff base compounds are one of the most efficient and environmentally benign corrosion inhibitors for the corrosion of metals by acids.[1−5] They stop metallic corrosion by obstructing the active areas on the metal surfaces. Their ability to inhibit this process is determined mainly by the chemical and structural characteristics of the Schiff base compounds. Functional group imine (−CH═N−) with numerous hetero atoms, like N, O, and S, are present in the overall structure of the Schiff base. Therefore, these can simply form a monolayer and adhere to the surface of the metal using hetero atoms. Hydrazones are used as rodenticides, nematicides, pesticides, insecticides, and plant growth regulators. Hydrazones are regarded as multidentate ligands because of their ability to chelate, just like Schiff bases. Compared to uncomplexed ligands, complexes of hydrazones with transition metal ions may exhibit increased antimicrobial activity.

Different organic additives can be used as corrosion inhibitors commonly known as ecofriendly dissolution inhibitors. However, some work has been done on the C-steel corrosion inhibition in an acidic environment. The corrosion of C-steel in acid media was investigated earlier in the presence of ornidazole,[2b] *Punica granatum* (pomegranate),[3] marjoram (*Origanum majorana*),[4] and *N*′-(4-hydroxybenzylidene)-2-(4-oxoquinazoline-3(4*H*)-yl) acetohydrazide [*p*-HBOA],[5] some new surface active agents.[6] But some aspects make hydrazone-based Schiff bases novel and potentially influential as corrosion inhibitors for C-steel: the hydrazone chemical structure provides various sites for interaction with metal surfaces. Nitrogen and oxygen atoms in the hydrazone group facilitate adsorption on the metal surface. Nitrogen atoms also increase the electron density, enhancing the interaction between the inhibitor and the metal surface. This interaction may form a stable protective film on the metal, inhibiting corrosion. Hydrazones exhibit electron donor properties, which can form coordinate bonds with metal ions on the metal surface. This coordination can block active sites on the metal, reducing the corrosion rate. The specific structure of hydrazones may introduce steric hindrance, affecting the adsorption process on the metal surface. Steric hindrance can influence the orientation and arrangement of the inhibitor molecules, leading to improved effectiveness.[6−9]

Considering the above facts, this research aims to develop renewed anticorrosive, sustainable, eco-friendly compounds for today's chemists and technology specialists. On this basis, galvanostatic techniques investigated three new Schiff base hydrazones as corrosion inhibitors against the C-steel surface in 8 M H_3PO_4. We measured the limiting current value and the mass transfer rate to assess how the hydrazones affected the rate of C-steel dissolving in orthophosphoric acid. By the way, numerous academics claim that the most valuable instruments for examining the effectiveness of metal corrosion inhibitors are quantum-chemical methods. DFT and Fukui's indices act as quantitative structure−activity relationships between inhibitors' inhibition efficiency and quantum chemical parameters. They also do not need lengthy experimental studies. They are used to verify that the results of computational chemistry research on the impact of mass transfer on the corrosion process of C-steel are consistent with experimental data. AAS was used to verify hydrazones' effect on the surface of C-steel, UV−visible, SEM/EDX, reflectance, and AFM.

EXPERIMENTAL SECTION

Preparation of Corrosive Environment (Medium) and C-Steel Specimens. The aggressive phosphoric acid solution, H_3PO_4 85% (SLRO/0450/PB17 Fisher Chemicals Ltd.), was a stock solution that had been diluted with clean, mineral-free water 8 M H_3PO_4 and the chosen of this concentration is based on previous research.[3] Then, the diluted phosphoric acid (8 M) was used to produce a range of concentrations by mole for use with different hydrazone inhibitors, taking molecular weight into account. The concentration range of inhibitors used was ($4.95−99.00 \times 10^{-3}$ mol/L). The experiments were triple-checked to ensure that the measurements were precise, and the outcomes were under 2% error. The three measurements are averaged to provide the stated corrosion results.

Electrodes were physically polished with several grades of silicon carbide sheets (P150), cleaned with distilled water, and degreased with acetone to remove the unwanted layer from the C-steel specimen. Epoxy glue was used to cover the cathode and anode's backs and the anode's surface, except (2×3 cm^2), which represents the dimension of the C-steel specimen used in galvanostatic measurements. The wt % structure was C = 0.14, Si = 0.03, Mn = 0.56, P = 0.02, Ni = 0.01, Cr = 0.01, V = 0.01, Al = 0.03, S = 0.04, and Fe = 99.15. Data were provided by European Corrosion Supplies Ltd. (U.K.).[9]

Galvanostatic Measurements. Since the galvanostatic method is both straightforward and reliable, it may become the standard method for determining an inhibitor's efficacy. The polarization experiments in the present investigation were carried out using the established procedures that were previously published.[3,9]

Synthesis of Hydrazone Inhibitor Molecules. *E-2-(1-Hydrazonoethyl)thiazole (HTZ).* To a solution of 1-(thiazol-2-yl)ethan-1-one (20 mmol, 2.54 g) in 50 mL of ethanol, 10 mL of hydrazine hydrate (50−60%) was added dropwise, and the resulting mixture was sonicated for 60 min at 60 °C. A white solid was produced with a yield of over 90% after the used solvent was evaporated under a vacuum and extra ether was added. Chemical formula: $C_5H_7N_3S$; ^{1}H NMR (400 MHz, $CDCl_3$) δ 7.70 (d, J = 3.1 Hz, 1H), 7.18 (s, 1H), 5.61 (brs, 2H), 2.23 (s, 3H). ^{13}C NMR (101 MHz, $CDCl_3$) δ 169.36, 143.20, 142.71, 119.71, 10.74 (Figures S1 and S2).[10]

https://doi.org/10.1021/acsomega.4c00199
ACS Omega 2024, 9, 16469−16485

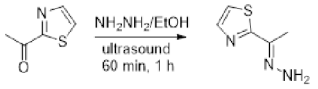

1-(thiazol-2-yl)ethan-1-one *E*-2-(1-hydrazonoethyl) thiazole **(HTZ)**

2-((E)-(((Z)-1-(Thiazol-2-yl)ethylidene)hydrazono)methyl)-phenol (HTZS). **HTZ** (705 mg, 5 mmol) and salicylaldehyde (610 mg, 5 mmol) were blended with two drops of AcOH (acetic acid) and 50 mL ethanol. Instantaneous product precipitation was followed by 60 min of sonication of the reaction mixture at 60 °C. After a few days of evaporation in air, the filtrate cooled to ambient temperature and crystallized into a light yellow block shape. ^{1}H NMR (400 MHz, $CDCl_3$) δ 11.70 (s, 1H), 11.37 (s, 1H), 8.69 (d, J = 11.7 Hz, 1H), 7.91 (dd, J = 13.5, 3.3 Hz, 1H), 7.43 (dd, J = 8.1, 3.5 Hz, 1H), 7.40−7.30 (m, 2H), 7.02 (dd, J = 8.4, 4.9 Hz, 1H), 6.95 (t, J = 7.5 Hz, 1H), 2.63 (s, 3H, CH_3); ^{13}C NMR (101 MHz, $CDCl_3$) δ 168.17, 167.57, 164.88, 164.75, 162.26, 160.27, 159.90, 157.68, 143.84, 133.55, 132.67, 122.67, 122.42, 119.90, 119.77, 117.84, 117.37, 117.20, 14.93 (Figures S3, S4).[11]

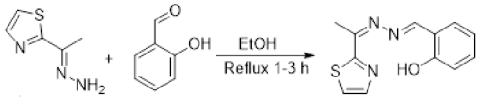

HTZ salicylaldehyde 2-((*E*)-(((*Z*)-1-(thiazol-2 yl)ethylidene)hydrazono) methyl)phenol **(HTZS)**

2-((E)-(((Z)-1-(Pyridin-2-yl)ethylidene)hydrazono)methyl)-phenol (HPYS). After adding 1.5 mL hydrazine hydrate (50−60%) dropwise to a 1-(4,5-dihydro thiazol-2-yl) ethan-1-one (20 mmol, 2.42 g) solution in 50 mL ethanol, it was sonicated at 60 °C for 60 min. A greater yield (>90%) of white solid was obtained when a vacuum was used to remove the solvent, and then an excessive amount of ether was added.

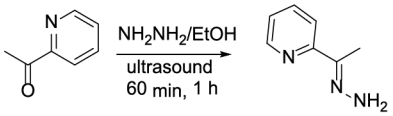

2-acetylpyridine 2-acetylpyridine hydrazone

2-Acetylpyridine 2-Acetylpyridine Hydrazone. In 50 mL of ethanol and 2 drops of AcOH (acetic acid), we combined 1620 mg, 12 mmol of 2-acetylpyridine hydrazone and 1464 mg, 12 mmol of salicylaldehyde. Instantaneous product precipitation was followed by 60 min of sonication of the reaction mixture at 60 °C. Light-yellow block-shaped crystals appeared in the filtrate after a few days of letting the solution slowly evaporate into the air at ambient temperature.[12]

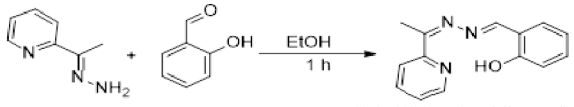

2-acetylpyridine hydrazone salicylaldehyde 2-((*E*)-(((*Z*)-1-(pyridin-2-yl)ethylidene)hydrazono) methyl) phenol **(HPYS)**

Spectroscopic Studies. *Atomic Absorption Spectroscopy (AAS).* The test C-steel sheets were inclined in 8 M H_3PO_4 as corrosive media without and with hydrazones (**HTZ, HTZS,** and **HPYS**) at different concentrations and temperatures (293−313 K) for 10 min. Quantitative measurement of Fe^{2+} was carried out using an atomic absorption spectrometer to measure the concentration of the acid (ANALYTIK JENA CONTRAA 300 Atomic Absorption). Galvanostatic polarization (GP) experiments were performed to quantify and compare the concentration of ferric ions remaining in solution.

Surface Analysis. Atomic force microscopy (AFM) equipped with a silicon nitride probe type MLCT from Bruker and operated in contact mode is used to assess the surface roughness of the materials. Parameters for the scan were adjusted in Proscan v 1.8 software. Contact mode, 25 × 25 μm^2 scan area, 1 Hz scan rate, 256 × 256 data points, and IP 2.1 software were used for this scan.

The specimen's reflection spectra and surface brightness degree of the C-steel were deliberated via UV−visible reflectance spectroscopy (Jasco V-570) in the 200−800 nm range.

The alterations on the C-steel surface following corroding and inhibiting were discovered by using scanning electron microscope (SEM). Micrographs taken with scanning electron microscopy revealed an intensive corrosion assault and the process of coating metal with a protective layer. Electron dispersion X-ray spectroscopy (EDX) was also used to show that the composition of the metal surfaces had changed. A JEOL JSM-IT200 microscope was utilized to capture the SEM and EDX micrographs.

Using ultraviolet−visible absorption spectrophotometry [Pg instruments *t*-80 UV−visible spectrophotometer], we analyzed the compounds' corrosive restricting capability with and without C-steel sample immersion in the restricting solution at optimum concentration [99.0 × 10^{-3} mol/L at 293 K of inhibin]. This gave us a better understanding of how the hydrazone inhibitors under study interact with the C-steel substrates.

Theoretical Approach. DFT calculations were performed in Gaussian-09 for this investigation.[13] The theoretical method was treated via a B3LYP/6-311G (d,p) basis set to provide reliable hydrazone geometries and electrical characteristics. The calculations were performed in the gas phase to demonstrate the connection between the molecular characteristics of hydrazones and their effectiveness as inhibitors. Due to its precision when using chemical principles, DFT can give a useful understanding of chemical reactions theoretically and selectivity like electronegativity (χ), hardness (η), softness (σ), and electrophilicity index (ω), in addition to other regional markers of reactivity, such as Fukui functions $f(r)$.

DFT is used to find out things like the highest filled and lowest free molecule orbital energies (E_{HOMO} and E_{LUMO}), which are known as values for the molecular orbital energies at the periphery (FMO), a gap of energy ($\Delta E_{gap} = E_{LUMO} - E_{HOMO}$), moment dipole ($\mu_d$), global electronegativity (χ), ionization energy (I), electron affinity (A), global softness (σ), chemical potential (P_i), global electrophilicity (ω), global

https://doi.org/10.1021/acsomega.4c00199
ACS Omega 2024, 9, 16469−16485

hardness (η), electroaccepting (ω^+) power, electrodonating (ω^-) power, the back-donation energy ($\Delta E_{b\text{-}d}$), fraction of transferred electrons (ΔN), and metal/inhibitor interaction energy ($\Delta E_{steel/inh.}$) using the equations.[14]

$$I = -E_{HOMO} \quad A = -E_{LUMO}$$

$$\eta = -\chi \qquad \chi = (I + A)/2 \quad \eta = (I - A)/2 \tag{1}$$

$$\sigma = 1/\eta \tag{2}$$

$$P_i = -\chi \tag{3}$$

$$\omega = P_i^2/2\eta \tag{4}$$

$$\Delta E_{b.d} = (-\eta)/4 \tag{5}$$

The following equation calculates the fraction of transferred electrons (ΔN):

$$\Delta N = \frac{(\chi_{Fe} - \chi_{hyd.})}{2(\eta_{Fe} + \eta_{hyd.})} = \frac{(\phi_{Fe} - \chi_{hyd.})}{2(\eta_{hyd.})} \tag{6}$$

where (χ_{Fe}, η_{Fe}) and ($\chi_{hyd.}$, $\eta_{hyd.}$) are, respectively, the electronegativity and chemical hardness of iron and the hydrazone inhibitor when ϕ_{Fe} is the function. In our research, the theoretical values of electronegativity ϕ_{Fe} = 7 eV and η_{Fe} are neglected as η of the bulk metals is linked to the opposite of the number of states they have at the Fermi level; it is a very minimal amount (equal zero).[15] C-steel/hydrazone inhibitor interaction strength ($\Delta\psi_{steel/inh.}$) is mathematically defined using the following formula:[16]

$$\Delta\psi_{steel/inh.} = \frac{(\chi_{Fe} - \chi_{Hyd.})^2}{4(\eta_{Fe} + \eta_{Hyd.})} \tag{7}$$

To determine the electrodonating potential of a substance, two novel global markers of chemical reactivity have been developed (ω^-) and electroaccepting (ω^+) powers (eq 8), which signify, in turn, a molecule's capacity to give and receive a very little quantity of charge.

$$\omega^- = \frac{(3I + A)^2}{16(I - A)}, \qquad \omega^+ = \frac{(I + 3A)^2}{16(I - A)} \tag{8}$$

In addition, the idea of net electrophilicity ($\Delta\omega^{\pm}$) was recently suggested by El-Mokadema et al.,[17] which measures and compares a molecule's electrophilicity in relation to its original nucleophilicity. Eq 9 was employed to compute this parameter.

$$\Delta\omega^{\pm} = \{\omega^+ - (-\omega^-)\} \quad \text{or} \quad \Delta\omega^{\pm} = \left\{\omega^+ - \left(\frac{1}{\omega^-}\right)\right\} \tag{9}$$

Additionally, the inhibitors under study had their molecular electrostatic potential (MEP) examined. For each atom in the molecules, the local softness $\sigma_k^{\pm}$ (σ_k^+ and σ_k^-) and local electrophilicity $\omega_k^{\pm}$ (ω_k^+ and ω_k^-) were also computed and connected to nucleophilic and electrophilic assaults, respectively, to understand better the active centers using the following equations.[18,19]

$$\sigma_k^{\pm} = \sigma f_k^{\pm} \tag{10}$$

$$\omega_k^{\pm} = \omega f_k^{\pm} \tag{11}$$

$$\Delta\sigma_k = \sigma_k^+ - \sigma_k^- = \sigma\Delta f_k \tag{12}$$

$$\Delta\omega_k = \omega_k^+ - \omega_k^- = \omega[\Delta f_k] \tag{13}$$

Also, by utilizing Yao's dual descriptor, the Fukui parameters [eq 14] allow us to determine whether an atom is electrophilic or nucleophilic.

$$\left.\begin{aligned} f_k^+ &= q_k(N+1) - q_k(N) \quad \text{For nucleophilic attack} \\ f_k^- &= q_k(N) - q_k(N-1) \quad \text{For electrophilic attack} \\ \Delta f_k &= f_k^+ - f_k^- \end{aligned}\right\} \tag{14}$$

The charge on the k atoms in a molecule is determined by $q_k(N + 1)$ when an electron is accepted. While a molecule is in its neutral state, its k atoms have no charges [$q_k(N)$]; however, when it loses an electron, they have charges ($q_k(N - 1)$). The electrophilic and nucleophilic Fukui functions are denoted by f_k^+ and f_k^-, respectively.[20]

Results and Discussion. *Galvanostatic Polarization and Effect of Operating Conditions.* The limiting current value that determines the corrosion inhibition efficiency relies on the rate of mass transfer of Fe^{2+} ions from the diffusion layer to the bulk of the solution. The mass transfer rate depends on the geometry of the anode, the relative ionic movement, the physical properties of the electrolyte, and temperature.[3−9]

Figure 1a,b represents the galvanostatic polarization curves for C-steel in a solution of 8 M H_3PO_4 for blank and different concentrations of hydrazones. Accordingly, when the inhibitor is present, the corrosion-limiting current decreases and, consequently, diminishes the mass transfer. Table 1 indicates

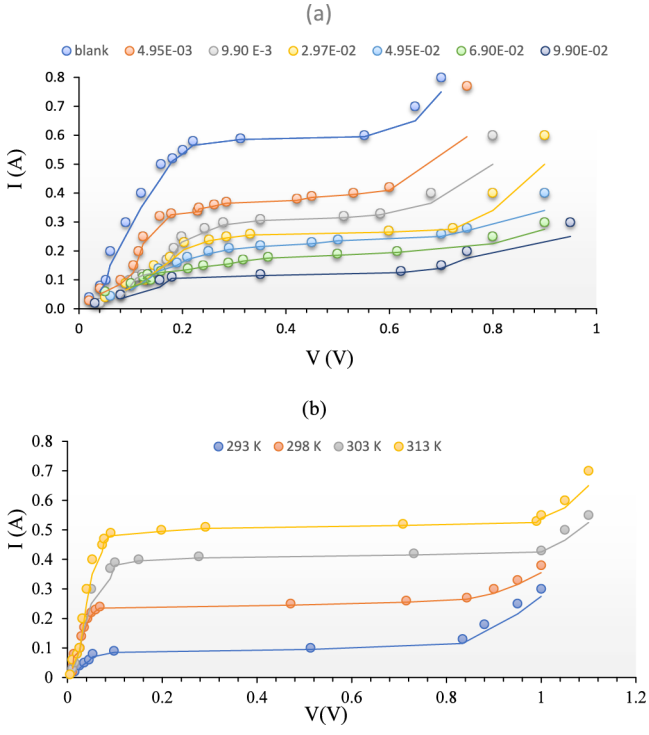

Figure 1. (a) Anodic polarization plots of C-steel electrode after exposure to various concentrations of **HTZ** at 293 K. (b) Anodic polarization plots of C-steel electrode with optimum concentration of **HTZS** (90.0×10^{-3} mol/L) at different temperatures.

https://doi.org/10.1021/acsomega.4c00199
ACS Omega 2024, 9, 16469−16485

Table 1. Calculated Limiting Current (A) and Inhibition Efficiency (I_{eff}%) in Galvanostatic Tests

		293 K		298 K		303 K		313 K	
hydrazones	$C_{hyd} \times 10^3$ mol/L	I_l	$\%I_{eff}$	I_l	$\%I_{eff}$	I_l	$\%I_{eff}$	I_L	$\%I_{eff}$
HTZ	blank	0.60	0.00	0.72	0.00	0.85	0.00	0.98	0.00
	4.95	0.38	36.60	0.53	26.38	0.75	11.76	0.89	9.18
	9.90	0.32	46.66	0.48	33.33	0.70	17.64	0.86	12.24
	29.70	0.27	55.33	0.42	41.66	0.65	23.52	0.76	22.44
	49.50	0.23	61.60	0.37	48.61	0.53	37.64	0.70	28.57
	69.30	0.19	68.33	0.32	55.55	0.49	42.35	0.67	31.63
	99.00	0.12	80.00	0.27	62.50	0.44	48.23	0.55	43.87
HTZS	blank	0.60	0.00	0.72	0.00	0.85	0.00	0.98	0.00
	4.95	0.33	45.00	0.49	31.94	0.72	15.29	0.87	11.22
	9.90	0.28	53.33	0.42	41.66	0.65	23.52	0.81	17.34
	29.70	0.24	58.53	0.39	45.83	0.56	34.11	0.69	29.59
	49.50	0.22	63.30	0.35	51.38	0.51	40.00	0.66	32.65
	69.30	0.17	71.66	0.30	58.33	0.47	44.70	0.61	37.75
	99.00	0.10	83.33	0.25	65.27	0.42	50.58	0.52	46.93
HPYS	blank	0.60	0.00	0.72	0.00	0.85	0.00	0.98	0.00
	4.95	0.42	30.00	0.56	22.22	0.77	9.40	0.90	8.16
	9.90	0.35	41.60	0.50	30.55	0.73	14.11	0.86	12.24
	29.70	0.30	50.00	0.49	31.94	0.69	18.80	0.80	18.36
	49.50	0.26	56.66	0.45	37.50	0.57	32.94	0.73	25.51
	69.30	0.21	65.00	0.40	44.44	0.53	37.64	0.69	29.59
	99.00	0.16	73.33	0.34	52.77	0.46	45.88	0.59	39.79

Table 2. Adsorption Isotherm Models of the Hydrazones with Values of R^2, Slopes, Intercept, K_{ads}, ΔG_{ads}, ΔH_{ads}, and ΔS_{ads} Obtained by Using Data from Measurements

adsorption isotherm model	linear form equation	hydrazones	T (K)	Y	intercept	R^2	K_{ads}	ΔG_{ads} (kJ mol^{-1})	ΔH_{ads} (kJ mol^{-1})	ΔS_{ads} (J mol^{-1} K^{-1})
Langmuir	$\frac{C_{hyd}}{\theta} = \frac{1}{k} + C_{hyd}$	HTZ	293	1.1998	0.0132	0.9770				
			298	1.4751	0.0200	0.9820				
			303	1.6683	0.0479	0.9405				
			313	1.8817	0.0653	0.9210				
kinetic–thermodynamic	$\log \frac{\theta}{1-\theta} = \log K + y \log C_{hyd}$		293	0.5582	1.0221	0.9150	67.77	−20.05	−93.83	−245.7
			298	0.5210	0.6977	0.9764	21.83	−17.59		
			303	0.6432	0.5909	0.9681	8.29	−15.45		
			313	0.6511	0.4717	0.9809	5.30	−14.79		
Langmuir	$\frac{C_{hyd}}{\theta} = \frac{1}{k} + C_{hyd}$	HTZS	293	1.1729	0.0111	0.9735				
			298	1.4673	0.0143	0.9814				
			303	1.7608	0.0290	0.9897				
			313	1.8493	0.0438	0.9674				
kinetic–thermodynamic	$\log \frac{\theta}{1-\theta} = \log K + y \log C_{hyd}$		293	0.3682	0.7633	0.9249	118.31	−21.41	−99.82	−269.8
			298	0.4079	0.6155	0.9325	32.28	−18.56		
			303	0.5531	0.5579	0.9938	10.00	−15.97		
			313	0.6093	0.5221	0.9880	7.19	−15.58		
Langmuir	$\frac{C_{hyd}}{\theta} = \frac{1}{k} + C_{hyd}$	HPYS	293	1.2776	0.0156	0.9806				
			298	1.7999	0.0252	0.9528				
			303	1.7636	0.0525	0.9802				
			313	2.0504	0.0737	0.9046				
kinetic–thermodynamic	$\log \frac{\theta}{1-\theta} = \log K + y \log C_{hyd}$		293	0.5579	0.9168	0.9543	43.98	−19.00	−91.21	−248.31
			298	0.4228	0.3887	0.9145	8.30	−15.19		
			303	0.6848	0.5616	0.9552	6.60	−14.87		
			313	0.6254	0.3740	0.9767	3.96	−14.04		

the values of the corrosion limiting current [i_{Lim}], and inhibition efficiency [$\%I_{eff}$]. Eq 15 is used to calculate the $\%I_{eff}$:

$$\%I_{eff} = \{[i_{Lim(a)} - i_{Lim(hyd)}]/i_{Lim(a)}\} \times 100 \quad (15)$$

where $i_{Lim(a)}$ is the limiting current without an inhibitor, and the limiting current when hydrazones are present is denoted as $i_{Lim(hyd)}$.

When compared to values obtained in the presence of varied hydrazone concentrations, i_{Lim} was maximum at all temperatures in the blank acidic solution. Increasing the reaction temperature enhanced the i_{Lim} at all doses of the inhibitors tested. The inhibitory efficiency of hydrazone decreased from 293 to 313 ± 1 K in 8 M H_3PO_4, as seen in Table 1. As temperature rises from 293 to 313 ± 1 K, more metal is dissolved. The protective coating may not be able to withstand

https://doi.org/10.1021/acsomega.4c00199
ACS Omega 2024, 9, 16469−16485

prolonged contact intervals due to a decrease in inhibitory effectiveness as temperature increases. Therefore, inhibiting corrosion at ambient temperature is preferred over higher temperatures. The adsorption/desorption equilibrium leans toward desorption, suggesting a physical adsorption process.[3]

Compared to the free solution, the corrosion rate was reduced when hydrazones were present. Inhibition is shown to be effective at higher hydrazone concentrations, where the hydrazone ions cause a thicker protective film to develop over the C-steel electrode.

Table 1 demonstrates that relative to the existence of an 8 M H_3PO_4 solution alone for Fe, the limiting current values (i_{Lim}) decrease and the efficiency of inhibition values ($\%I_{eff}$) increase as the concentration of the compounds under study increases. As the fraction of surface covering increases, θ (i.e., the proportion of the metal surface covered by the hydrazone molecules) is responsible for the concentration-dependent improvement in inhibitory effectiveness. Experimental data support the widespread belief that inhibitor molecules reduce corrosion by adsorbing to a metal's surface, forming a protective barrier layer and slowing down the substrate's corroding rate.[6,7]

Adsorption Considerations. When evaluating adsorption properties, knowledge about surface covering, which can be found by dividing the percentage blocking efficiency by 100, is essential. At a fixed temperature, the inhibitor content is tied to well-known equilibrium adsorption isotherm formulas. Langmuir and kinetic−thermodynamics adsorption isotherm models have been utilized.[3] The linearization form of these adsorption isotherms is illustrated in Table 2 and Figures 2 and 3.

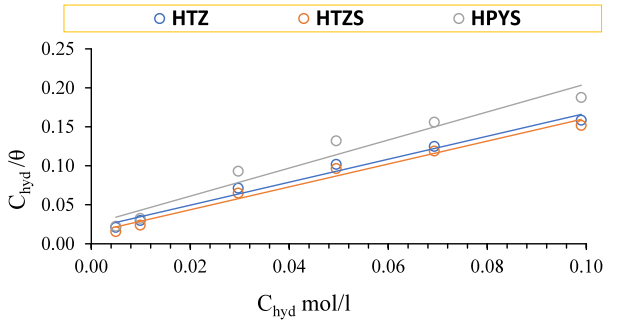

Figure 2. Variation of C_{hyd}/θ with C_{hyd} for the adsorption of hydrazones on a C-steel surface at 298 K.

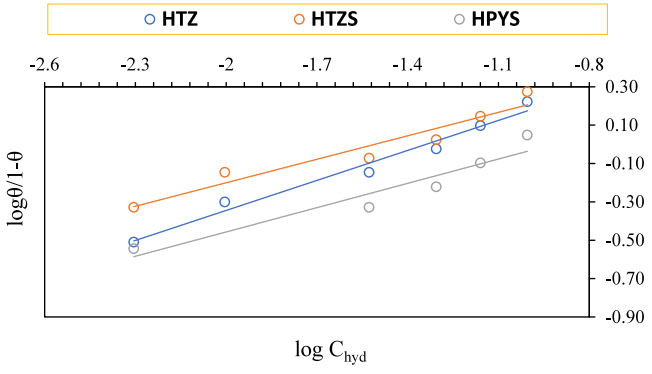

Figure 3. Variation of $\log \theta/1-\theta$ with $\log C_{hyd}$ for the adsorption of hydrazones on a C-steel surface at 298 K.

C_{hyd} is the inhibitor concentration, and K is the degree of adsorption. y is a constant related to adsorbed molecules, and K' is a constant ($K = K'^{1/y}$). Figure 2 makes it evident that C_{hyd}/θ and C_{hyd} have a linear connection with a slope that is not 1. This demonstrated that the capacity of hydrazones to stick to the surface of carbon steel did not follow Langmuir's absorption rule. According to the Langmuir model, adsorption takes place on many layers of the adsorbent, and homogeneous film formation occurs on the C-steel surface.[21]

From Figure 3 and Table 2, we can obtain values of $1/y$, which are beyond 1 and demonstrate that an inhibitor molecule takes up more than one active site. In other words, the K value increases if the inhibitor sticks to the metal surface better. In Table 2, the K values are displayed. Using the following equation, ΔG_{ads}, the adsorption-free energy was estimated:[22,23]

$$K = \frac{1}{55.5}\exp(-\Delta G_{ads}/RT) \tag{16}$$

As a constant, 55.5 stands for the molar concentration of water in the solution; the adsorption parameters are shown in Table 2. Inhibitor molecules strongly contacting metal surfaces and spontaneously adhering to them are referred to by the negative sign of the ΔG_{ads}. Thus, physical adsorption is the basis for the adsorption heat values utilized here (often, physical adsorption may be reached with ΔG_{ads} values of up to −20 kJ mol^{-1}.[24] From eq 17, the enthalpy of adsorption (ΔH_{ads}) and entropy of adsorption (ΔS_{ads}) were obtained.

$$\Delta G_{ads} = \Delta H_{ads} - T\Delta S_{ads} \tag{17}$$

The linear relation between ΔG_{ads} versus T gives ΔS_{ads} (−ve of the slope) and ΔH_{ads} (intercept of the line with the y-axis). Since adsorption is exothermic (heat is given off) and inhibitory efficacy decreases with temperature, we know that the enthalpy of adsorption is −ve. From Table 2, −ve values of ΔS_{ads} in 8 M H_3PO_4, the incorporation of inhibitors into the C-steel surface, and the driving force of the reaction may be slowed by decreasing the randomization from reactants to the metal/solution interface.

The value of $\Delta S_{ads} < 0$ shows that the instability decreases once the complex compound is created, allowing H_2O molecules to desorb from the surface. This indicates that the adsorption mechanism is stationary and that the complex compound creation is connected to the rate-determining phase. Enhancing K_{ads} values also offers substantial interactions between inhibitor chemicals and metallic surfaces.[25]

Dubinin−Radushkevich Isotherm Model (D−RIM). D−RIM was used to discriminate between physical and chemical adsorption; it can be expressed as:[24]

$$\ln \theta = \ln \theta_{max} - a\delta^2 \tag{18}$$

where θ_{max} is the maximum surface coverage, and δ is the Polanyi potential, it can be correlated as

$$\delta = RT \ln(1 + 1/C_{hyd}) \tag{19}$$

C_{hyd} is the amount of inhibitor present in g/l. The plots of $\ln \theta$ versus δ^2 are shown in Figure 4; isotherm constant values (a) and the largest possible area covered (θ_{max}) may be calculated from the isothermal slopes and intercepts. All of the corresponding parameters are listed in Table 3. Furthermore, the isotherm constant (a) has something to do with the average free energy of the adsorbate molecules, E_m, where 1

https://doi.org/10.1021/acsomega.4c00199
ACS Omega 2024, 9, 16469−16485

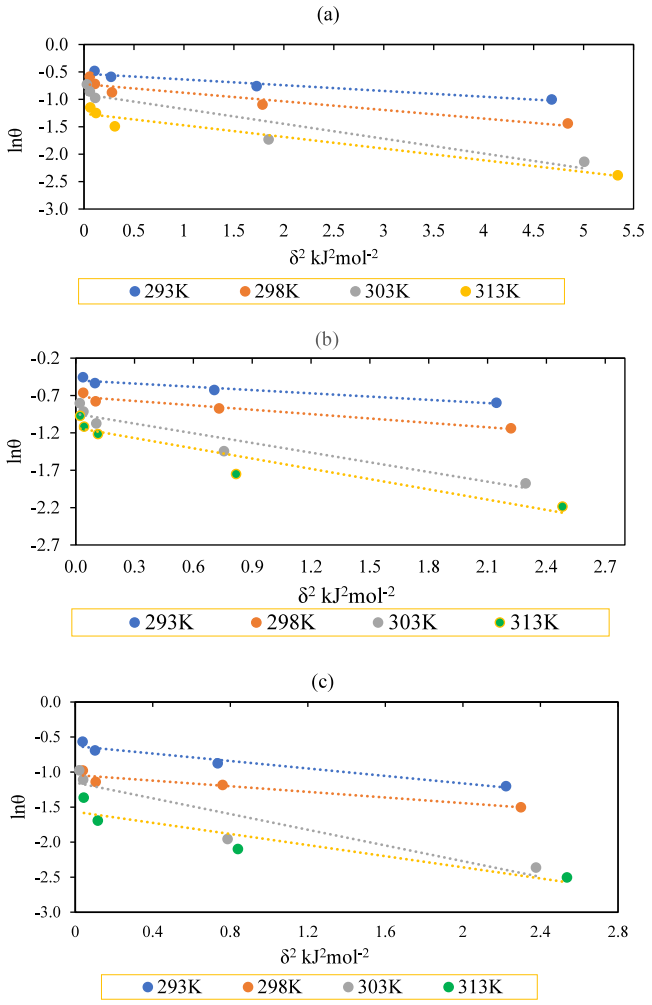

Figure 4. Dublin−Radushkevich isotherm for the adsorption of (a) **HTZ**, (b) **HTZS**, and (c) **HPYS** on C-steel surfaces at different temperatures and concentrations.

Table 3. Some Linear Regression Parameters from the Dubinin−Radushkevich Isotherm Model for Hydrazone Adsorption on a C-steel Surface in 8 M H_3PO_4 at Different Temperatures

hydrazones	T (K)	R^2	a (kJ^{-2} mol^2)	θ_{max}	E_m (kJ mol^{-1})
HTZ	293	0.9500	0.1046	0.5866	2.1860
	298	0.9041	0.1568	0.4851	1.7857
	303	0.8930	0.2706	0.4041	1.3590
	313	0.9532	0.2122	0.2831	1.5350
HTZS	293	0.9448	0.1456	0.6088	1.8530
	298	0.9543	0.1953	0.4893	1.6000
	303	0.9146	0.4315	0.3879	1.0765
	313	0.9050	0.4578	0.3226	1.0450
HPYS	293	0.9588	0.2666	0.5332	1.3695
	298	0.9240	0.2006	0.3527	1.5788
	303	0.8605	0.5066	0.3166	0.9935
	313	0.8649	0.3968	0.2089	1.1225

mol of adsorbate transferred from infinity (bulk solution) to the adsorbent surface energy as

$$E_m = 1/(2a)^{1/2} \quad (20)$$

The magnitude of E_m provides details about the adsorption type that has been observed. Figure 5 shows D−RIM for the

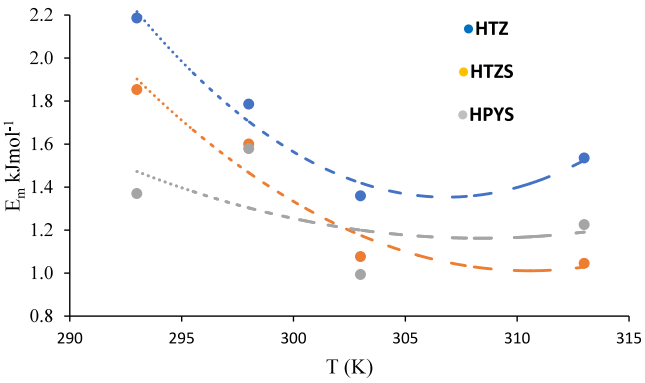

Figure 5. Mean adsorption energy vs temperature for hydrazones on C-steel.

adsorption of hydrazones on the C-steel surface. Values of R^2 obtained from the plots reveal that D−RIM applies to hydrazones' adsorption on the C-steel surface. E_m is an index for predicting the mechanism of the adsorption of the inhibitor. When E_m is less than 8 kJ/mol, a physical adsorption mechanism is upheld and vice versa. According to our previous results, the numerical values of E_m reflect the physical adsorption mechanism.

Activation Parameters. By charting a graph of ln i_{Lim} vs $1000/T$, the activation energy (E_a) for different amounts of hydrazones in 8 M H_3PO_4 was calculated. The resultant plotting curve (Figure 6) gives a straight line with slopes to permit the calculation of E_a by applying the following equation:[27]

$$i_{Lim} = A\, e^{(E_a/RT)} \quad (21)$$

where A is the reaction's frequency factor, R is the universal gas constant, and T is the temperature in Kelvin. Table 4 shows the expected value of E_a for the C-steel in hydrazones. Table 4 shows that the E_a values are greater when hydrazones are present than when they are not, suggesting physical adsorption. Electrostatic binding has been said to be the reason for this kind of success.[28] The rise in E_a in the system where rust is stopped shows that the energy barrier for corrosion is getting higher. In the presence of inhibitors, the estimated E_a suggests that the contact between the metal surface and the studied inhibitors was strong enough to make it hard for the acid to attack the metal surface, implying that corrosion was stopped.

Adsorption of hydrazones on the C-steel surface can be exothermic or endothermic depending on the reaction condition, the nature of hydrazone molecules, and the mechanism of the reaction. For more proof, you can get an idea of the heat of adsorption (Q_{ads}) by looking at how the amount of surface covering changes with temperature:[29,30]

$$\log\left(\frac{\theta}{1-\theta}\right) = \log A + \log C - \left(\frac{Q_{ads}}{2.303RT}\right) \quad (22)$$

where A is a constant, Figure 7 shows the plot of the $\log\left(\frac{\theta}{1+\theta}\right)$ as a function of $\frac{1000}{T}$. The adsorption of hydrazone species on the Fe surface is an exothermic process associated with a high negative value of adsorption heat (Q_{ads} = −67.15, −73.13, and

https://doi.org/10.1021/acsomega.4c00199
ACS Omega 2024, 9, 16469−16485

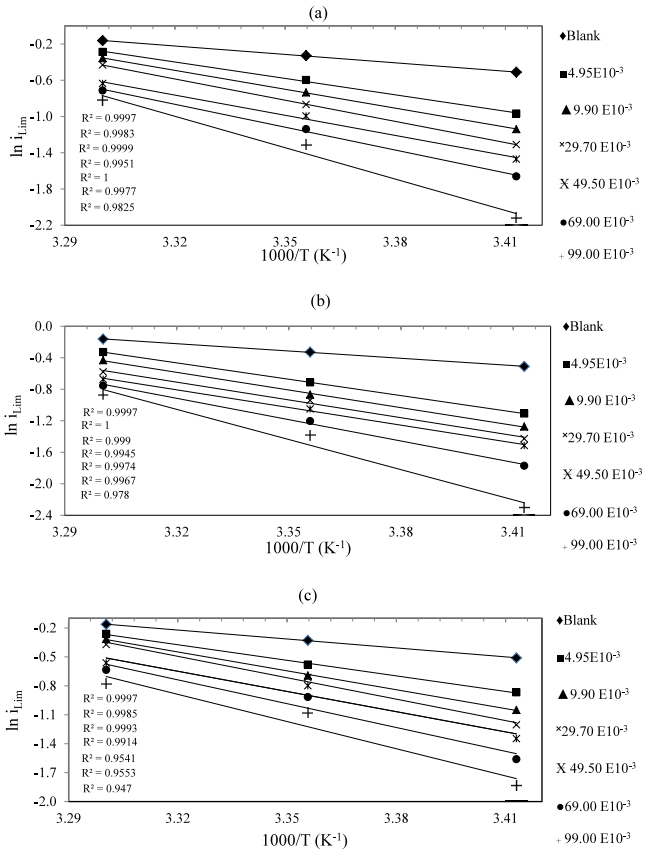

Figure 6. Arrhenius relation for corroded C-steel under several concentrations of (a) **HTZ**, (b) **HTZS**, and (c) **HPYS**.

Table 4. Activation Parameters of the Corroded C-steel in 8 M H_3PO_4 Inhibitor-Free Solution in the Presence of Different Concentrations of Hydrazones

hydrazones	E_a (kJ/mol)	Q_{ads} (kJ/mol)	ΔS^* (J/mol K)	ΔH^* (kJ/mol)	ΔG^* (kJ/mol)
Blank	18.50		−194.21	15.96	75.29
HTZ	31.79	−67.15	−152.02	29.27	75.15
	37.20		−134.93	34.69	75.40
	39.01		−129.93	36.50	75.72
	41.40		−123.22	38.89	76.08
	47.11		−105.26	44.60	76.36
	55.37		−79.79	52.86	76.94
HTZS	36.57	−73.13	−136.83	34.06	75.35
	40.36		−125.29	37.85	75.65
	39.12		−130.50	36.61	75.99
	41.01		−124.92	38.50	76.20
	47.54		−104.48	45.03	76.55
	59.62		−66.46	57.11	77.17
HPYS	29.01	−63.14	−160.91	26.50	75.05
	34.09		−144.85	31.59	75.30
	36.06		−138.97	33.55	75.49
	37.08		−136.64	34.57	75.80
	42.68		−119.03	40.17	76.09
	43.91		108.14	43.91	76.55

−63.14 kJ mol^{-1}), so the physical absorption process that was suggested before is clear-cut.[3]

The usual equation of the transition state was used to determine changes in (ΔH^*) enthalpy and (ΔS^*) activation entropy.

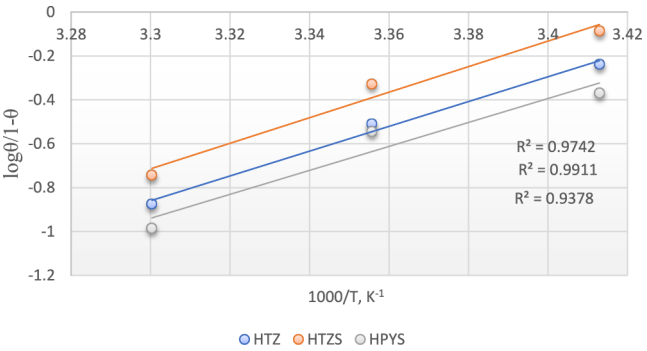

Figure 7. Plot of log $\theta/1-\theta$ with $1000/T$ (K^{-1}) for C-steel in 8 M H_3PO_4 in the absence and presence of hydrazones (4.95×10^{-3} M).

$$\ln i_{Lim}/T = [\ln R/Nh + \Delta S^*/R] - \Delta H^*/RT \quad (23)$$

where N denotes Avogadro's number, and h represents the Planck constant. The linear relationship between $\ln(i_{Lim}/T)$ against $1000/T$ gives a slope of $-\Delta H^*/R$, ΔS^* = {intercept − $\ln(R/Nh)$}R, and the parameters of enthalpy and entropy are reported in Table 4.

The rise in hydrazone concentration causes a hike in ΔH^*, which indicates that the endothermic nature has increased. Adsorption of molecules on C-steel surfaces inhibits working active sites. Hydrazones enhance entropy factors' (ΔS^*) activation during the rate-determining phase, reducing disorder from the activated complex to the reactants.[31]

Solution Composition Analysis. *Atomic Absorption Spectroscopy (AAS) Measurements.* As an indirect measurement method, atomic absorption spectroscopy (AAS) is regarded as an optical atomic spectrometric approach that focuses on the concentration (amount) of iron ions (Fe^{2+}) in the corrosive solution produced by the corrosion of C-steel in an acidic environment. Figure 8 and Table 5 show the

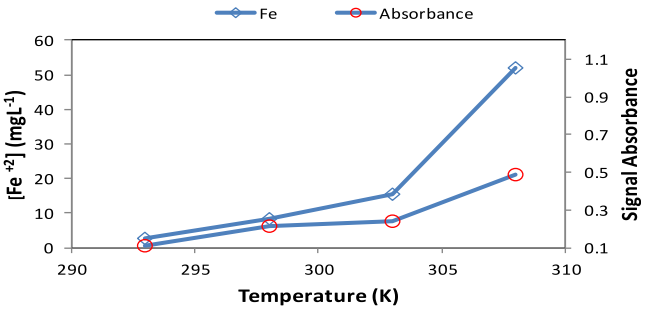

Figure 8. Concentration and absorbance of dissolved Fe^{2+} ions in the solution as a function of temperatures.

absorption, the percentage of inhibition efficiency (%IE_{AAS}), and the amounts of the iron metal ions left in the solution after galvanostatic polarization (GP). The method for figuring out the %IE_{AAS} is

$$\%IE_{AAS} = \left(1 - \frac{C_{hyd}}{C^*}\right) \times 100 \quad (24)$$

C^* and C_{hyd} are the amounts of iron dissolved in the fluid with and without inhibitors, respectively. When the hydrazones (**HTZ**, **HTZS**, and **HPYS**) were present, less iron metal ions were left in the 8 M H_3PO_4 solution after rusting than when the inhibitors were not present, according to an analysis of the

https://doi.org/10.1021/acsomega.4c00199
ACS Omega 2024, 9, 16469−16485

Table 5. Depict the AAS Study of Dissolved Ferrous (Iron) Ions in Corroding Solution Against 8 M H_3PO_4 Control Under Different Temperatures and Concentrations of Hydrazones

samples	$[Fe^{2+}]$ (mg· L^{-1})	signal absorbance	$\%IE_{AAS}$
iron + 8 M H_3PO_4 (293 K)	112.10	0.73932	-
iron + 8 M H_3PO_4 (298 K)	127.30	0.75806	-
iron + 8 M H_3PO_4 (303 K)	144.20	0.94251	-
iron + 8 M H $_3PO_4$ (313 K)	164.40	1.07050	-
iron + 8 M H_3PO_4 + 4.95×10^{-3} mol/L HTZ (303 K)	31.20	0.38210	78.36
iron + 8 M H_3PO_4 + 4.95×10^{-3} mol/L HTZS (303 K)	15.40	0.24291	89.32
iron + 8 M H_3PO_4 + 4.95×10^{-3} mol/L HPYS (303 K)	42.20	0.42953	70.74
iron + 8 M H_3PO_4 + 99.0×10^{-3} mol/L HTZS (303 K)	23.60	0.31233	83.63
iron + 8 M H_3PO_4 + 4.95×10^{-3} mol/L HTZS (303 K)	15.40	0.24291	89.32
iron + 8 M H_3PO_4 + 4.95×10^{-3} mol/L HTZS (293 K)	2.70	0.10959	97.59
iron + 8 M H_3PO_4 + 4.95×10^{-3} mol/L HTZS (298 K)	8.40	0.21575	93.40
iron +8 M H_3PO_4 + 4.95×10^{-3} mol/L HTZS (303 K)	15.40	0.24291	89.32
iron + 8 M H_3PO_4 + 4.95×10^{-3} mol/L HTZS (313 K)	51.90	0.48697	68.43

data in the last table. This finding proves that adding inhibitors to the aggressive H_3PO_4 solution had the desired effect of slowing the rate of iron metal corrosion. With a $\%IE_{AAS}$ of 89.32%, **HTZS** demonstrated the highest corrosion inhibition efficiency of the three inhibitors tested. At 303 K, **HPYS** was the least effective at stopping corrosion with a rate of 70.74%. The values of inhibition efficiency percentage that can be estimated from the dissolution rate and the AAS method agree well.[32−34]

UV−Visible Responding Complexes. UV−visible spectroscopy can be used to analyze adsorption on the surface of the C-steel to observe the dissolution of iron (Fe^{2+}) and validate the formation of the iron/inhibitor complex. This was explained by the difference between the wavelength λ_{max} of an 8 M H_3PO_4 corrosive solution with and without hydrazones. Figure 9 demonstrates the UV−visible absorption spectra for the blank, with the optimum concentration of the three hydrazones before and after coating with C-steel. By analyzing spectra, it is possible to see how pure inhibitor inhibit C-steel sample absorbance values and intensities differ when compared to blank sample. It is also interesting to note that the peak of the blank solution, which was seen at 235 nm, is weaker than those of the three inhibitor solutions. Strong evidence for improved interaction between inhibitors and acidic media is shown by the wavelength values λ_{max} of pure inhibitors mixed with H_3PO_4 traveling to higher values of 250, 245, and 240 nm for **HTZS, HTZ**, and **HPYS**, respectively. Two events happened following metal exposure, as shown in the diagram. The peak positions for **HTZS**, **HTZ**, and **HPYS** were slightly shifted to 245, 240, and 238 nm, respectively, to correspond to $\pi-\pi^*$lone pair electron transmissions with a minor reduction in the absorbance's intensity. According to the literature,[35,36] a shift in the location of the absorbance maximum and the absorbance value in an inhibited solution are signs that a complex between the metal ions and the inhibitor has formed. So, the hydrazones−Fe^{2+} complex acts as a barrier that effectively protects the surface of the C-steel from corrosive H_3PO_4 solution attack.

Corrosion Appearance Analysis. *Corrosion Attack Morphology and Elemental Analysis (SEM and EDX).* The inhibitory potential and potential creation of the protective barrier by the investigated molecules on the C-steel surface were assessed by using quantitative EDX studies and qualitative microscopic SEM investigations to validate the galvanostatic tests. The C-steel morphology of steel samples is shown in before (Figure 10A), after (Figure 10B), and with and without hydrazones (Figure 10C−F). According to the images, the steel coupon in Figure 10A has a rough surface, cavities, clear pits, and porous layers packed with tiny fractures before submerging in an 8 M H_3PO_4 solution devoid of inhibitor.

In turn, the chemicals can readily corrode the plate by penetrating the steel.[36,37] The C-steel surface in Figure 10b is exceedingly rough, with thick, uneven layers covering the surface when exposed to a very powerful solution without inhibitors (blank). The presence of a strong oxygen peak in the C-steel EDX spectra of the blank makes it obvious that corrosion-induced processes produce iron oxide (rust). The presence of the phosphorus peak, which indicates the existence of this element on the surface because it originates from the 8 M H_3PO_4 solution in the solution, should also be seen following immersion in a strongly acidic solution. The SEM image shows that the C-steel surface with hydrazone inhibition appears undisturbed.[38,39]

The C-steel surface becomes less harmed than the blank by adding 4.95×10^{-3} mol/L **HTZS** (Figure 10C), and some larger pores and cracks are created on the surface. The C-steel surface (Figure 10D) becomes extremely smooth and corrosion-free as the concentration of **HTZS** (99.0×10^{-3} mol/L) increases. Steel is less likely to dissolve when **HTZS** is used under corrosive conditions because it generates an extremely uniform adhesive layer on the metallic surface. This shows that the inhibitor's corrosion resistance was improved at increasing concentrations. Adding 99.0 $x10^{-3}$ mol/L inhibitors of **HTZ** and **HPYS** significantly reduces iron dissolution and surface damage, as shown in Figure 10E,F, compared to the blank solution (Figure 10B). These can be compared to find that the test materials' surface smoothness is on the order of **HTZS** > **HTZ** > **HPYS**. It is evident that the samples' surfaces have an effective protective coating that prevents corrosion.

The metallic surface exposed to unrestricted acidic media produced specific indications for oxygen, iron, and carbon, according to EDX analysis. Even though the metallic surface exposed to hydrazone-inhibited acidic medium exhibits the same signals, the intensity of the oxygen signal is diminished, there is a notable decrease in the phosphorus peak, and there is an increase in the appearance of the nitrogen peak when compared to raw and blank. These findings support the anticorrosion effect of hydrazones by demonstrating that oxide production is reduced when they are present. This indicates the compounds' inhibitory capabilities since they can block electrolyte access and minimize the corrosion phenomenon by forming a protective layer on the surface of the C-steel.

AFM. The primary measure utilized to assess localized corrosion activity and the kinetics of the corrosion of metallic materials was surface visualization of the surface topography. AFM analysis was done to examine the surface morphology thoroughly, and the results are shown in Figure 11. It is easy to see how the surface morphology has changed with the

https://doi.org/10.1021/acsomega.4c00199
ACS Omega 2024, 9, 16469−16485

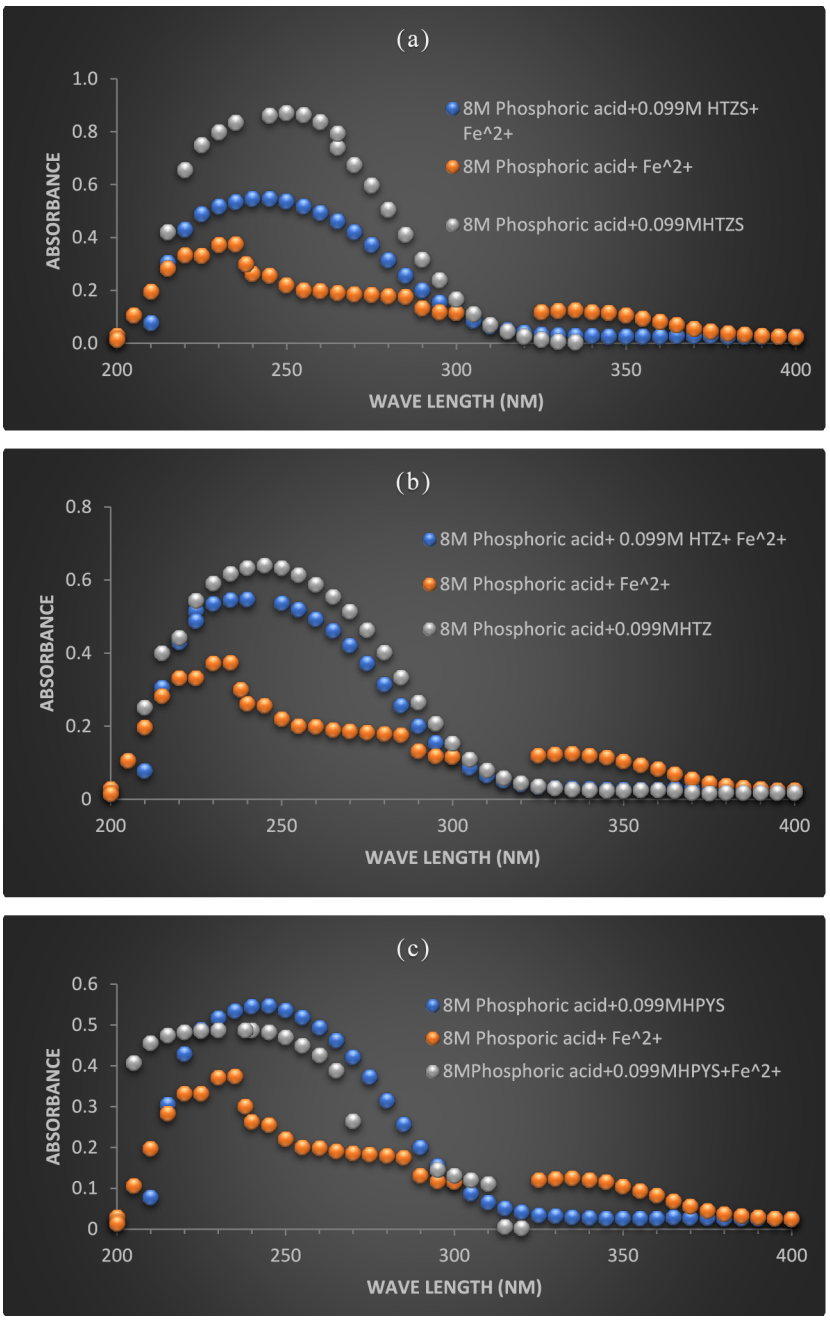

Figure 9. UV−visible spectra of 8 M H_3PO_4 free solution, containing 99.00 × 10^{-3} M of (a) **HTZS**, (b) **HTZ**, and (c) **HPYS** before and after the test with a C-steel electrode.

performance of different inhibitors in corrosion protection. The hydrazone's adsorbed layer was visualized by AFM and characterized by roughness parameters (Figure 11). The resistance of the C-steel surface to the corrosive environment was analyzed and represented by 3D-dimensional AFM images (Figure 11a−c). The C-steel 3D images without adding hydrazones reveal that the metal surface was damaged severely because of the corrosive attack of the 8 M H_3PO_4 (Figure 11b) and the peaks and valleys around 4.31 μm. However, adding hydrazones to the corrosive medium reduces the aggressive medium's corrosive attack, as shown in Figure 11d−f, with smooth surfaces.

The valleys and peaks are located at 1.01 μm (**HTZS**), 1.74 μm (**HTZ**), and 2.03 μm (**HPYS**). The AFM data further support the order of the inhibitory efficiency discovered by electrochemical measurement experiments. Also, Table 6 compares the Ra and Rq parameters, which are usually used to describe the surface roughness of solids, which were decreased from 0.213 and 0.301 μm to 0.088 and 0.119 μm upon increasing the concentration of **HTZS** from 4.95 x10^{-3} mol/L to 99.0 × 10^{-3} mol/L (59% and 60% reduction), respectively.

The smoothest surface roughness was obtained in the C-steel sample with **HTZS**, which is about 0.088 and 0.119 μm, and the maximum surface roughness belongs to **HPYS**, which equals 0.206 and 0.283 μm, respectively. One could conclude that tiny delamination and microcracks significantly impact surface roughness measurement.

https://doi.org/10.1021/acsomega.4c00199
ACS Omega 2024, 9, 16469−16485

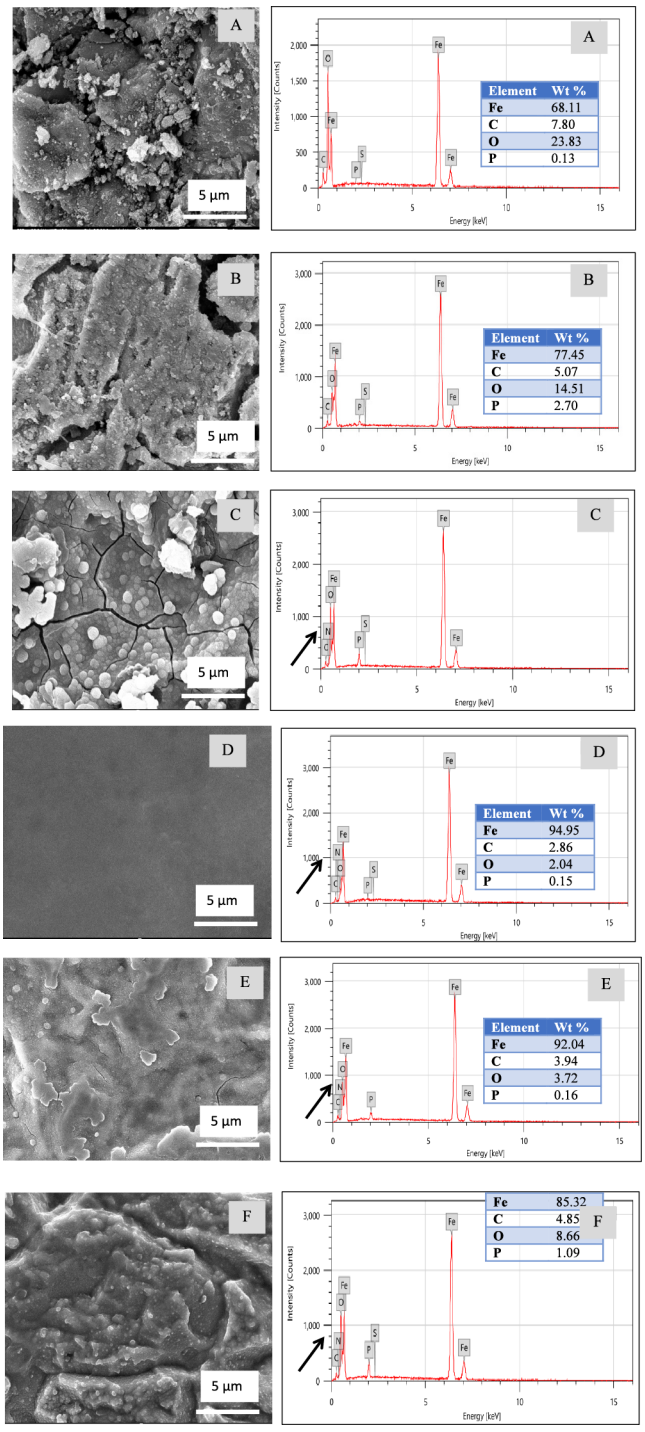

Figure 10. SEM, EDX spectra, and EDX parameters for C-steel in the uninhibited and inhibited media at 293 K: (A) raw, (B) blank, (C) **HTZS** 4.95 × 10^{-3} mol/L, (D) **HTZS** 99.0 × 10^{-3} mol/L, (E) **HTZ** 99.0 × 10^{-3} mol/L, and (F) **HPYS** 99.0 × 10^{-3} mol/L.

Additionally, the surface grains were growing larger, and the dome-shaped surface grains' diameter was increasing. These findings utterly validate the SEM image results and their widespread praise. The section on brightness measurements that follows will provide more evidence that roughness measures support scanning electron microscope pictures.[40,41]

UV Spectral Reflectance Studies (Gloss Value). Improvements in the circumstances used, such as inhibitor type, concentrations of the electrolytic solution, and temperature, significantly impact the brightness and smoothness of the C-steel surface under corrosion by the aggressive. There is a strong inverse association between the brightness and surface roughness. The gloss of C-steel surfaces in the company of hydrazones increases with decreasing roughness, as indicated in Table 6. It is known that when Rp-v rises, brightness drops, and light scatters when it is reflected.

According to this investigation, the reflectance (gloss value) gradually increases for the specimen dipped in an 8 M H_3PO_4 solution and is the lowest for raw C-steel samples. The production of thin films on the metal surface may cause these variations in gloss value. The reflectance percentage of the inhibitor-used specimens is higher than that of the blank sample. This demonstrates that the development of a coating on the surface has resulted in a further alteration of the surface properties.

Due to an increase in the inhibitor's adsorption, the reflectance percentage rose as the inhibitor concentration did. Figure 12a displays reflectance curves for specimens corroded, dipped in a blank solution, and at various inhibitor doses. Additionally, several samples revealed a decline as the inhibitor type changed (Figure 12b).[42−44]

Computational Details. To acquire a deeper understanding of the mechanism of corrosion inhibitors on metal surfaces, we looked into the relationship between the electronic structure and inhibition mechanism of hydrazone molecules in neutral forms under gas phase circumstances using DFT. The FMOs and the global reactivity descriptors generated from quantum mechanical calculations for describing the I_{eff} (%) structural characteristics were used to assess the anticorrosion potentials of hydrazones. HOMO, LUMO, and electrostatic potential maps of the inhibitors are shown in Figure 13.

As shown in Figure 13, hydrazones may interact with the corroding C-steel surface in acidic solutions via heteroatoms and π-electrons, which may function as nucleophilic adsorption centers and $\pi-\pi$ stacking, resulting in the expected inhibitory mechanism. The optimized shape of the B3LYP/6-31G (d,p) displays the tested inhibitors' active centers.

In general, the ability of a compound to donate electrons to LUMO acceptors is determined by the energy of HOMO (E_{HOMO}). In contrast, a molecule's ability to accept electrons depends on the energy of the LUMO (E_{LUMO}) orbital. As the energy gap value (ΔE) decreased, the energy required to remove an electron from the HOMO orbital (excitation energy) decreased, which increased the ability of compounds to adsorb on the surface of the metal. As a result, electrons were readily donated to the Fe atom's vacant d-orbital,[45] resulting in a stable inhibitor metal complex with improved inhibition abilities. Table 7 demonstrates that the energy gap values were in the following order: **HTZS** < **HTZ** < **HPYS**. It has been suggested that a molecule with a smaller energy gap may be more polarizable. Soft molecules are those with low kinetic stability and strong chemical reactivity.

Additionally, scientists noted that the site of the molecules with the largest global softness (σ) is where inhibitor molecules adsorb onto the surface of the C-steel. It is evident that **HTZS** has the highest degree of softness and, hence, the greatest ability to protect the surface of the C-steel, which is consistent with experimental findings.[16−18] The interaction between C-steel and hydrazone inhibitor molecules is related to the ionization energy (I) and electron affinity (A) of produced inhibitors.[17]

https://doi.org/10.1021/acsomega.4c00199
ACS Omega 2024, 9, 16469−16485

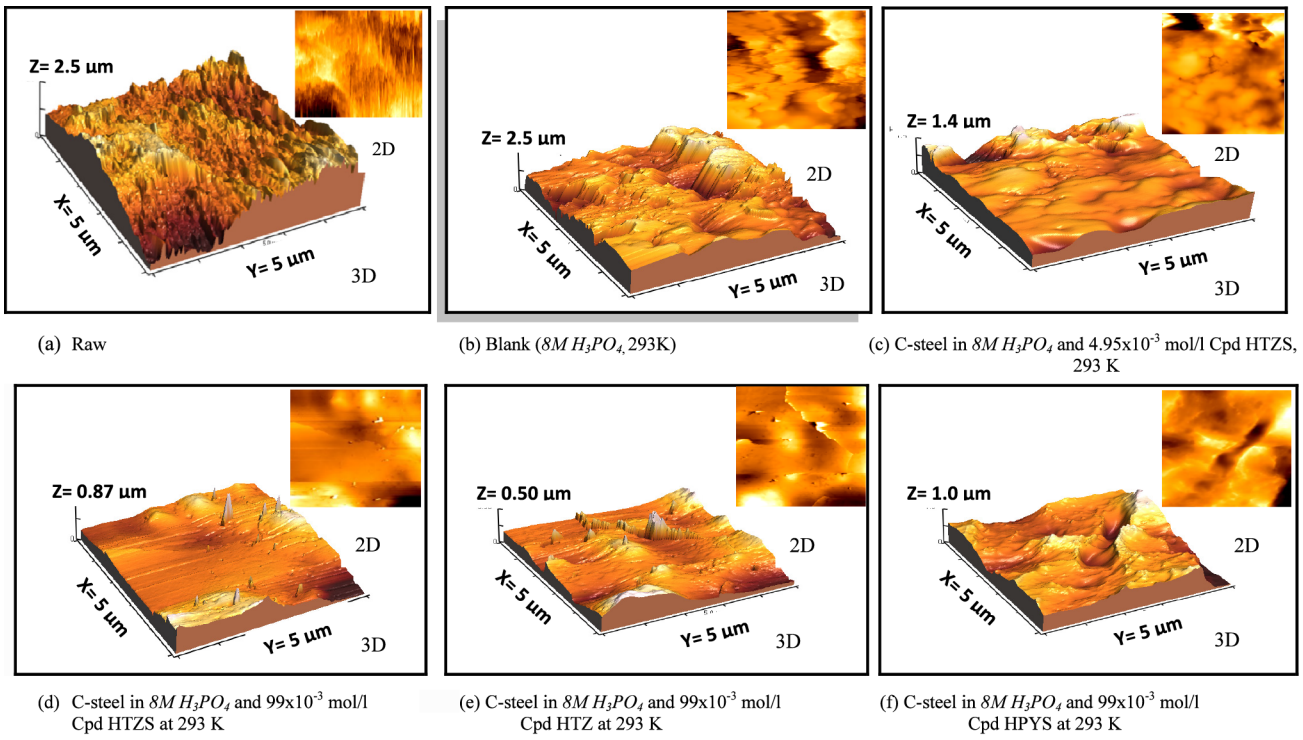

Figure 11. 2D and 3D roughness profiles for the C-steel scanned area with hydrazones.

Table 6. Change of Gloss Values and Roughness Parameters of C-Steel after Exposure to the Corroded 8 M H_3PO_4 Free Solutions and under Optimum Hydrazone Concentrations at 293 K

corrosion conditions	brightness (gloss value)	Rq [μm]	Ra [μm]	Rp-v [μm]	%I_{eff}
raw sample	16.30	0.789	0.624	4.99	-
after corrosion without additives	27.70	0.364	0.468	4.31	0.00
after corrosion with 4.95×10^{-3} mol/L of HTZS	43.40	0.301	0.213	2.79	53.33
after corrosion with 99×10^{3} mol/L of HTZS	137.20	0.119	0.088	1.01	83.33
after corrosion with 99×10^{-3} mol/L of HTZ	77.60	0.138	0.098	1.74	80.00
after corrosion with 99×10^{-3} mol/L of HPYS	54.60	0.283	0.206	2.03	73.33

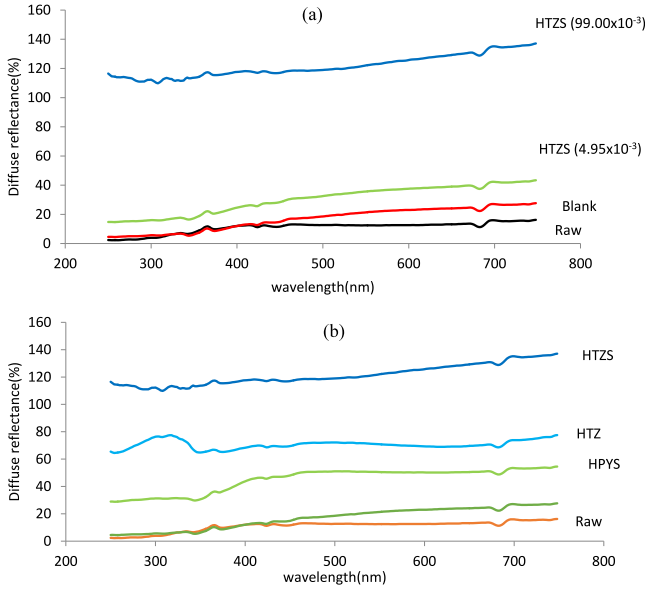

Figure 12. (a) Effect of **HTZS** concentrations on the gloss value of C-steel samples at temperature 293 K. (b) Effect of inhibitor type on measured gloss value (G) of C-steel samples at the concentration (99.00×10^{-3} M) and temperature 293 K.

Recently, some authors have utilized the dipole moment to measure the effectiveness of molecules' ability to inhibit corrosion, where the dipole moment's magnitude increases the inhibition's effectiveness. The process of transporting electrons is made more accessible by the increasing value of the dipole moment. Others, however, suggested the opposite relationship, stating that a low value of dipole moment favors the aggregation of inhibitor molecules on the surface of the C-steel, improving the inhibitory performances. The computed dipole moments for the examined hydrazones agree with the second suggestion, as shown in Table 7. However, the review of the literature[26] reveals a number of irregularities in the relationship between dipole moment and inhibitor effectiveness. Therefore, in general, there is no noteworthy correlation between the magnitudes of the dipole moment and the efficacies of inhibition.[46−48]

This outcome, therefore, motivated us to explore the researched systems' accepting and donating properties further. The effectiveness of the hydrazones' experimental inhibition and their ability to give and/or take electrons were compared using three models for this purpose: (i) the electrodonating (ω^-) and the electroaccepting (ω^+) powers, proposed by Gázquez et al.,[50] (ii) the net electrophilicity index ($\Delta\omega^{\pm}$) (Chattaraj et al.),[51] and (iii) the back-donation ($\Delta E_{b\text{-}d}$)

https://doi.org/10.1021/acsomega.4c00199
ACS Omega 2024, 9, 16469−16485

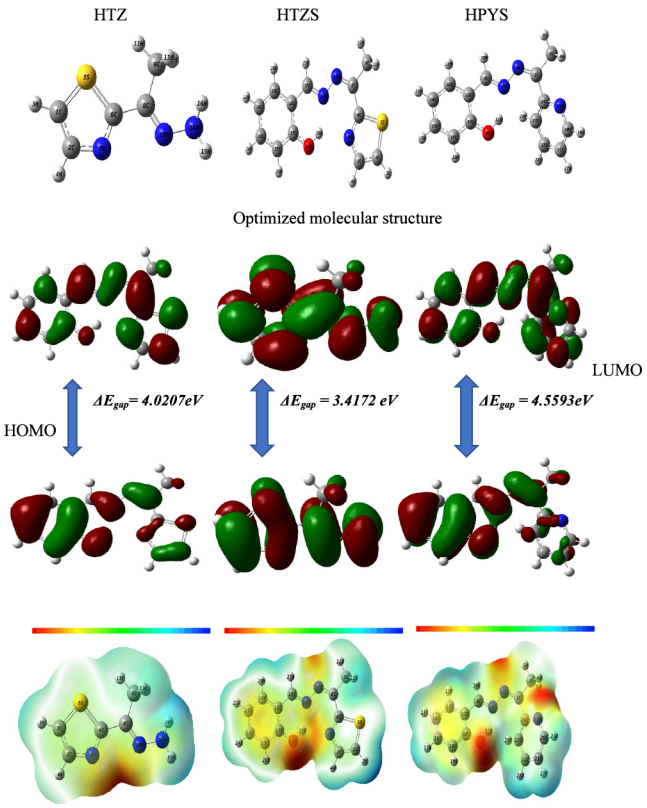

Figure 13. Optimized structures, frontier molecular orbitals, and ESP distribution of the hydrazone molecules calculated using the B3LYP/6-311G (d,p) method.

Table 7. Calculated Molecular Electronic Structure Parameters of Studied Prepared Hydrazones in Neutral Form in the Gas Phase

hydrazone inhibitors	HTZS	HTZ	HPYS
E_{HOMO} (eV)	−5.8580	−6.1078	−5.9457
E_{LUMO} (eV)	−2.4409	−2.0871	−1.3864
ΔE_{gap} (eV)	3.4172	4.0207	4.5593
I	5.8580	6.1078	5.9457
A	2.4409	2.0871	1.3864
χ	4.1494	4.0975	3.6661
P_i	−4.1494	−4.0975	−3.6661
μ_d (Debye)	1.7608	1.8486	2.6645
η (eV)	1.7086	2.0104	2.2797
σ (eV^{-1})	0.5853	0.4974	0.4387
ω (eV)	5.0386	4.1757	2.9478
ω^-	7.3271	6.4757	5.0658
ω^+	3.1776	2.3782	1.3997
$\omega^{\pm}$	10.5046	8.8539	6.4655
$\omega^{\pm}$	3.0411	2.2238	1.2023
$\Delta E_{b\text{-}d}$ (eV)	−0.4271	−0.5026	−0.5699
ΔN (eV)	0.8342	0.7219	0.7312
T.E (Hartee)	−1101.7303	−780.9610	−757.2583
%IE	83.33	80.00	73.33
$\Delta\psi_{steel/hyd.}$ (eV)	1.1889	1.0476	1.2189

(Martinez-Gomez et al.).[52] From the results in Table 7, the observed increase of the experimental inhibition efficiency results in the rise of ω^-, ω^+, $\Delta\omega^{\pm}$, and $\Delta E_{b\text{-}d}$ with increasing size of heteroatoms of researcher inhibitors. These findings support the conclusion that **HTZS** was the best inhibitor.

Inhibitor interactions with C-steel surfaces may be affected by the electronic back-donation process, as predicted by the simple charge transfer hypothesis for charge donation and back-donation.[47] According to eq 5, the energy shift is proportional to the inhibitor molecule's hardness when the electron transfer and back-donation processes occur concurrently. Therefore, the charge transfer from a molecule, followed by a back-donation to the molecule, is energetically favored, as shown by the $\Delta E_{b\text{-}d} < 0$ because $\eta > 0$. According to this concept, the inhibitor's effectiveness should rise when the molecule can better adsorb onto the metal surface. As the hardness increases, it stands to reason that $E_{b\text{-}d}$ will fall. As seen in Table 7, our computed $\Delta E_{b\text{-}d}$ has the following trend, which is consistent with the experimental results: **HTZS** > **HTZ** > **HPYS**.[16−18]

The global electrophilicity index represents the molecule's propensity to take electrons and quantifies the energy stabilization that occurs when a system gains ΔN electron charges from its surroundings. The current research shows that the global electrophilicity index, ω, correlates well with the corrosion inhibition effectiveness. Since **HTZS**'s electrophilicity index is the greatest of the three compounds, it stands to reason that it will also be the most potent nucleophile (donor).

Global electronegativity (χ) refers to the molecule's propensity to take in electrons. The negative heteroatoms (N, O, S) improve electronegativity, corrosion resistance, and inhibitor adsorption on the C-steel surface by boosting donor−acceptor interactions. This enhances the electrostatic contact between the C-steel and the inhibitor. Through a high electronegative C-steel (7 eV) − low electronegative hydrazone (Table 7) interaction, electrons migrate from the donor hydrazones to the acceptor C-steel until equivalency was achieved.[15]

The electronegativity/hardness equalization method may be used to generate ΔN as a descriptor. It was said that molecules play the role of electron donors if the number of electrons transferred (ΔN) is positive and the opposite if ΔN is negative. All ΔN values in this work are positive, indicating that molecules donate electrons during adsorption. When it comes to inhibiting corrosion, a larger ΔN suggests that the inhibitor is more likely to interact with the metal surface. Table 7 shows that **HTZS** has the highest net positive proportion of transferred electrons (ΔN), making it the most electron-rich molecule. The total energy (E) and starting energy ($\Delta\psi$) of the molecule−metal interaction (ΔN) are also crucial factors. The data show that **HTZS** has the greatest value of total energy (T.E) and is favorably adsorbed through active adsorption sites. Table 7 lists the computed values for the studied inhibitors $\Delta\psi$. However, in this research, the trend of ΔN and $\Delta\psi$ values does not match well with the trend of inhibition efficiency as assessed experimentally.[18]

Mullikan population analysis may be used to predict where the hydrazones' inhibitors will adsorb. The primary calculation is the charge distribution throughout the whole skeleton of the molecule. The atoms in the adsorbed core are more willing to donate an electron to the metal's unfilled orbital if they have a higher negative charge. Strong adsorption of the inhibitors on the C-steel surface is guaranteed by the presence of O, S, and N atoms as well as numerous electrons on these molecules. Table 7 lists the net charges on the atoms in the hydrazone (not including hydrogen atoms). Therefore, N, O, and certain C atoms have the greatest binding affinity to the C-steel

https://doi.org/10.1021/acsomega.4c00199
ACS Omega 2024, 9, 16469−16485

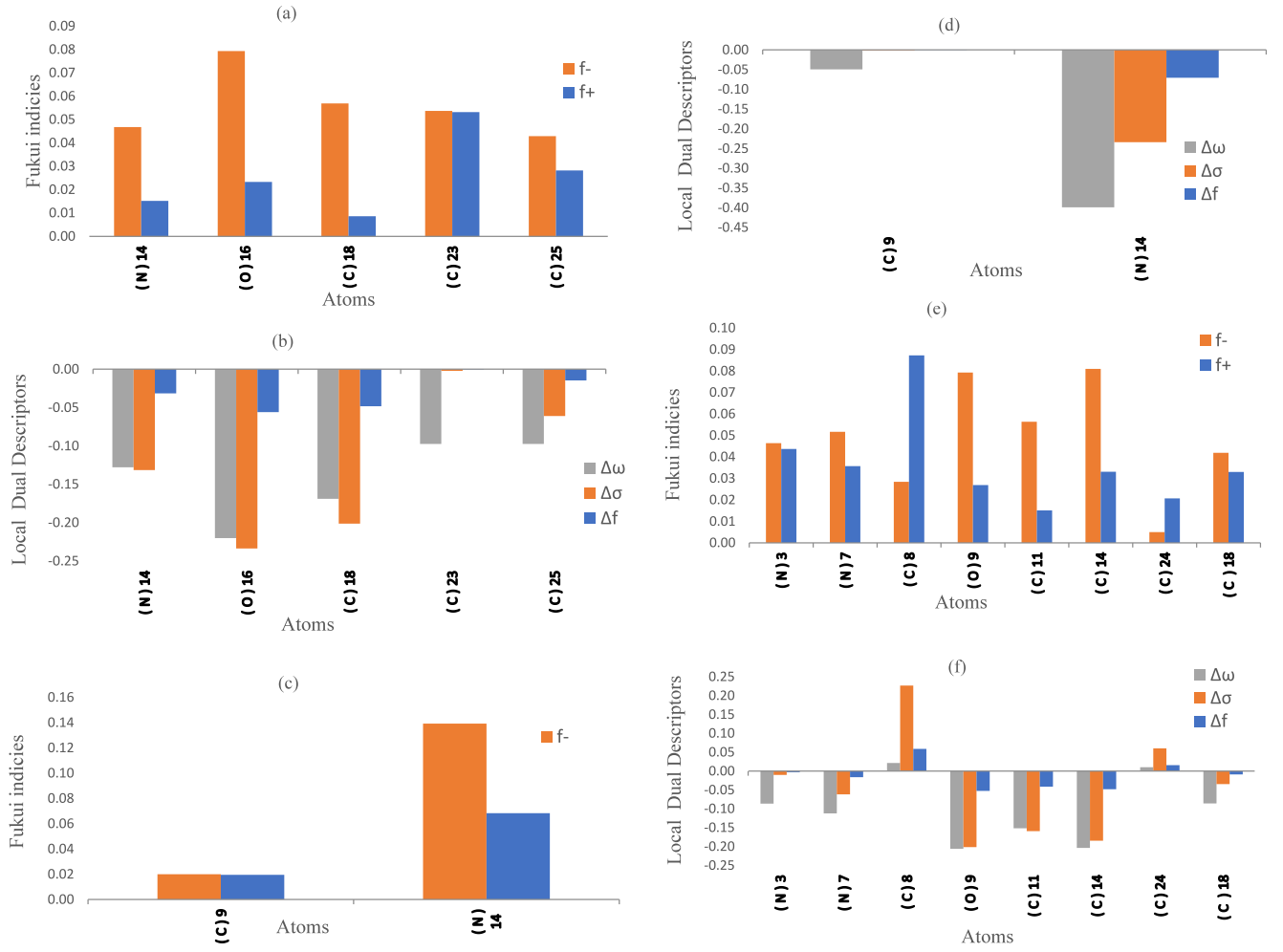

Figure 14. Graphical representation of the dual local descriptors and Fukui indices for selected atoms in the gas phase for (a, b) **HTZS**, (c, d) **HTZ**, and (e, f) **HPYS.**

surface and function as electron donors due to their role as active adsorption sites.

However, the inhibitor effectively interacts with a metal surface because certain C atoms have positive charges that nucleophiles will target. Therefore, this contact will slow the corrosion process. Molecular electrostatic potential (MEP) and Fukui indices corroborate this finding.

The electrophilic and nucleophilic reactivities may be inferred from the change in color of the areas of electron density in MEP, as shown in Figure 13, which helps to understand the adsorption process and detect the probable reactive sites of inhibitors. The positive (nucleophilic) and low-density (blue) regions indicate nucleophilic reactivity, whereas the negative (red) regions denote electrophilic reactivity. Red has the highest electron density, followed by orange, yellow, green, and blue. High electron-rich patches (yellow to red hue) were shown to be concentrated on (C9) and (N14) in **HTZ**; (C23), (C25), (C18), (N14), and (O16) in **HTZS**; and (C18), (C14), (C11), (N3), (N7), (O9), and (C18) in **HPYS**. For **HPYS**, C8 and C24 are the electron-poor locations (colored green to blue). In addition, as the MV of the hydrazones grows, so does the inhibitor's capacity to shield the C-steel surface. Thus, the S-containing heterocyclic compound often displays good corrosion inhibition performance due to the presence of high-density electron clouds around the substitutive atoms/groups on the ring,[46] which will generate an electronic interaction with the iron's vacant d orbitals and imply that adsorption between hydrazone molecules and the iron surface occurs spontaneously.[49]

Fukui indices are the appropriate method for investigating the nucleophilic and electrophilic local reactive sites responsible for an inhibitor's behavior. Table 7 and a line graph of Figure 14 show the results of calculating the condensed Fukui functions with Mulliken charges (f_k^+, f_k^-), local electrophilicity (ω_k^+, ω_k^-), and local softness (σ_k^+, σ_k^-). We calculated (Δf_k), which is equivalent to the difference ($f_k^+ - f_k^-$), to help us compare the relative attractiveness of sites for nucleophilic and electrophilic attacks on any given atom (k). If Δf is greater than zero, then the site is preferable for a nucleophilic attack, and if Δf is less than zero, then the site is preferable for an electrophilic attack.[3,9]

The tabulated results reported in Table S1 reveal, for the nucleophilic attack, the highest f_k^- values of Inh. **HTZS** N14, O16, C18, C23, and C25 atoms. For Inh. **HTZ**, the most nucleophilic sites are N14 and C9 atoms. For **HPYS**, the most reactive sites are N3, N7, O9, C11, C14, and C18. This demonstrates a tendency to form coordinating bonds with iron by donating electrons to empty molecular orbitals on the metal's surface. The findings from the calculated global reactivity are consistent with this. Out of the three investigated inhibitors, C8 and C24 in HPYS have the highest f_k^+ values for the electrophilic attack, suggesting that these sites are most

https://doi.org/10.1021/acsomega.4c00199
ACS Omega 2024, 9, 16469−16485

suited for an electrophilic assault in which the molecule takes electrons to form feedback bonds with the Fe surface. Local dual index values (Δf, $\Delta\sigma$, and $\Delta\omega$) corroborate these findings by pointing to a high concentration of active sites inside these inhibitors. Some atoms were discovered to have values greater than 0 for all three descriptors, however, suggesting that these centers are electrophilic (see Figure 14). In accordance with the frontier orbital results, a closer look at the molecular structures would reveal additional reactive sites that play a key role in increasing the reactivity of the investigated molecules, thereby enhancing interactions with the metal surface via a back-donation process.

These findings suggest that there will be several active sites in the Inh. **HTZS** molecule that may interact with the iron substrate. Bonding to the iron surface through electron donation to the Fe 3d orbitals[18] is more likely to occur at places containing N and O atoms. Furthermore, it is hypothesized that the binding between the metal's surface and the Inh. **HTZS** is more robust than those in the cases of **HTZ** and **HPYS**. In conclusion, the aforementioned regional descriptors show that the theoretical order for the change in inhibition efficiencies of the investigating inhibitors is as follows: **HTZS** > **HTZ** > **HPYS**, which agrees with the current experimental evidence.

Proposed Protection Mechanism. The adsorption of hydrazones on the C-steel surface may entail at least one of the following interactions, as shown by the aforementioned experimental and theoretical findings: the iron oxide coating has a positive surface charge; therefore, it attracts PO_4^{-3} ions when placed in an 8 M H_3PO_4 solution. Hydrazones are good inhibitor adsorbents because they contain either an electron aromatic ring or an electronegative donor atom (N, O, or S) or both. As a result, the electrostatic interaction between the positively charged molecules of the inhibitor and the negatively charged metal surface promotes the physical adsorption of the inhibitor onto the C-steel surface (Figure 15). After that, the

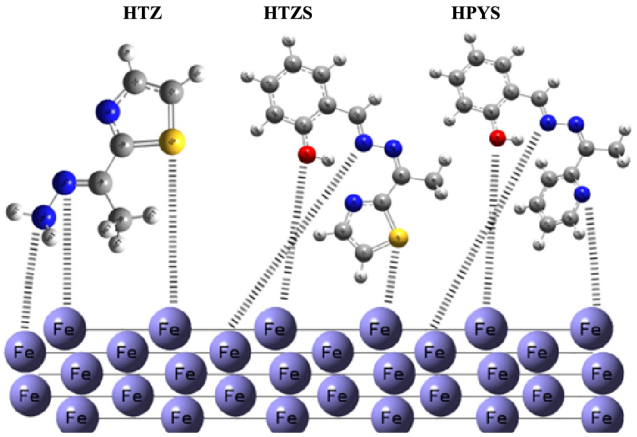

Figure 15. Schematic diagram for the C-steel corrosion inhibition process in the presence of hydrazones.

presence of these molecules protects the metal from the corrosive fluid. Additionally, the ionized Fe atoms on the surface interact with π-electron clouds on the aromatic ring through a donor−acceptor mechanism known as retrodonation. Also, on the other hand, it can be based on the size of the inhibitor molecule. The large surface area of the Inh. **HTZS,** due to the presence of S, N, and O atoms, allows for the creation of a larger surface due to the large molecular volume of atoms protecting against the corrosion process. This may be the primary reason that this compound has higher inhibitory characteristics than Inh. **HTZ** and **HPYS**, which are superior to previously reported inhibitors under the same conditions (Table S2)[3,9] The corrosion resistance of C-steel in acidic solutions might be improved by increasing the concentration of hydrazones. The barrier created for mass and charge transfer is achieved by increasing the surface covering and the amount of adsorbed inhibitor molecules. Therefore, the order of the hydrazones' $\%I_{eff}$ is **HTZS** > **HTZ** > **HPYS**, as predicted by the quantum chemical calculations and confirmed by the experimental study.[53,54]

CONCLUSION

- Galvanostatic experiments proved that a mass transfer mechanism was responsible for corrosion inhibition.
- Three hydrazones have been researched as C-steel 8 M H_3PO_4 solution corrosion inhibitors. They have effective corrosion inhibition.
- A maximum inhibition efficiency ($\%I_{eff}$) of 83.33% was attained using an optimum concentration of **HTZS** at 293 K.
- The physical adsorption of inhibitors, which obeys the kinetics adsorption isotherm, was observed.
- By applying the Dubinin−Radushkevich isotherm model, the numerical values of E_m confirm the physical adsorption mechanism.
- The UV−visible studies revealed complex formation, which may also be responsible for the observed inhibition.
- SEM, EDX, reflectance, and AFM morphology results indicated that forming a protective film on the C-steel surface protected it from corrosion in the 8 M H_3PO_4 solution.
- The findings from DFT and the Fukui indices correspond well with the experimental data.

ASSOCIATED CONTENT

Data Availability Statement

The data used and analyzed during the current study are available from the corresponding authors upon reasonable request.

Supporting Information

The Supporting Information is available free of charge at https://pubs.acs.org/doi/10.1021/acsomega.4c00199

Included the characterization of hydrazone Schiff bases *E*-2-(1-hydrazonoethyl) thiazole (**HTZ**) and 2-((*E*)-(((*Z*)-1-(thiazol-2-yl) ethylidene) hydrazono) methyl) phenol (**HTZS**) (^{1}H NMR, and ^{13}CNMR); tables for Fukui indices and compared the present work with the previous works (PDF)

AUTHOR INFORMATION

Corresponding Author

Amira H. E. Moustafa − *Chemistry Department, Faculty of Science, Alexandria University, Alexandria 0203, Egypt;* orcid.org/0000-0001-7670-1987; Email: amira.mostafa@alexu.edu.eg, amirahossameldin79@yahoo.com

https://doi.org/10.1021/acsomega.4c00199
ACS Omega 2024, 9, 16469−16485

Authors

Hanaa H. Abdel-Rahman − *Chemistry Department, Faculty of Science, Alexandria University, Alexandria 0203, Egypt*

Assem Barakat − *Chemistry Department, College of Science, Saudi Arabia, King Saud University, Riyadh 11451, Saudi Arabia;* orcid.org/0000-0002-7885-3201

Hagar A. Mohamed − *Laboratory Department, Faculty of Applied Health Sciences Technology, Pharos University, Alexandria 0203, Egypt*

Ahmed S. El-Kholany − *Laboratory Department, Faculty of Applied Health Sciences Technology, Pharos University, Alexandria 0203, Egypt*

Complete contact information is available at: https://pubs.acs.org/10.1021/acsomega.4c00199

Author Contributions

H.H. and A.H.E. finished the study design. A.B., A.H.E.M., and H.A. completed experimental studies. A.H.E., H.A. and A.S. finished the data analysis. A.H.E. and H. H. finished the manuscript editing. All authors read and approved the final manuscript.

Funding

No funds, grants, or other support was received.

Notes

The authors declare no competing financial interest.

■ ACKNOWLEDGMENTS

The authors gratefully acknowledge the employees working in the Electron Microscopy Unit, Faculty of Science, Alexandria University, and National Institute of Standards (NIS), Cairo, for their helpfulness in all characterization.

■ REFERENCES

(1) Kesari, P.; Udayabhanu, G. Investigation of Vitamin B_{12} as a corrosion inhibitor for mild steel in HCl solution through gravimetric and electrochemical studies. *Ain Shams Eng. J.* **2023**, *14*, 101920.

(2) (a) Damej, M.; Hsissouc, R.; Berisha, A.; Azgaoua, K.; Sadikud, M.; Benmessaoud, M.; Labjar, N.; El Hajjaji, S. New epoxy resin as a corrosion inhibitor for the protection of carbon steel C38 in 1M HCl: experimental and theoretical studies (DFT, MC, and MD). *J. Mol. Struct.* **2022**, *1254*, 132425. (b) Ikeuba, A. I.; Faithpraise, F. O.; Nwokolo, K. I.; Umo, F. E.; Echem, O. C.; Ibrahim, A. T.; Edet, H. O.; Ita, B. I.; Okafor, P. C.; Asogwa, F. C.; Amajama, J.; Iwuji, P. C. A combined electrochemical and DFT investigation of ornidazole as a benign anti-corrosion agent for carbon steel materials in acidizing environments. *Results Mater.* **2024**, *21*, 100542.

(3) Moustafa, A. H. E.; Abdel-Rahman, H. H.; Awad, M. K.; Naby, A. A. N. A.; Seleim, S. M. Molecular dynamic simulation studies and surface characterization of carbon steel corrosion with changing green inhibitors concentrations and temperatures. *Alex. Eng. J.* **2022**, *61*, 2492−2519.

(4) Taha, A. A.; Abouzeid, F. M.; Elsadek, M. M.; Othman, Y. M. The Electropolishing of C-Steel in Orthophosphoric acid containing Methanolic Plant Extract. *Alex. Eng. J.* **2022**, *61*, 4889−4909.

(5) Moustafa, A. H. E.; Seleim, M. S.; Abdel-Rahman, H. H.; Embaby, A. M.; Omar, A. Z. Functionalization Strategies for Electropolishing Process of Carbon Steel Using Novel Quinazoline-4-one Derivatives: Synthesis, Spectroscopic Characterization, and DFT Studies. *ACS Omega* **2023**, *8*, 30949−30965.

(6) Taha, A. A.; Shaban, S. M.; Fetouh, H. A.; Taha, S. T.; Sabet, V. M.; Kim, D.-H. Synthesis and evaluation of nonionic surfactants based on dimethylaminoethylamine: Electrochemical investigation and theoretical modelling as inhibitors during Electropolishing in-ortho-phosphoric acid. *J. Mol. Liq.* **2021**, *328*, 115421.

(7) Singh, D. K.; Ebenso, E. E.; Singh, M. K.; Behera, D.; Udayabhanu, G.; John, R. P. Non-toxic Schiff bases as efficient corrosion inhibitors for mild steel in 1 M HCl: Electrochemical, AFM, FE-SEM and theoretical studies. *J. Mol. Liq.* **2018**, *250*, 88−99.

(8) Tang, M.; Deng, S.; Du, G.; Li, X. *Mikania micrantha* extract/KI blend as a novel synergistic inhibitor for steel corrosion in concentrated H_3PO_4 solution. *Ind. Crops Prod.* **2023**, *193*, 116237.

(9) Moustafa, A. H. E.; Abdel-Rahman, H. H.; Mabrouk, D. F.; Omar, A. Z. Mass transfer role in electropolishing of carbon steel in H_3PO_4 containing amino acids: Electrochemical, computational, SEM/EDX, and stylus profilometer investigation. *Alexandria Eng. J.* **2022**, *61*, 6305−6327.

(10) Altowyan, M. S.; Khalil, S. M. S. M.; Al-Wahaib, D.; Barakat, A.; Soliman, S. M.; Ali, A. E.; Elbadawy, H. A. Synthesis of a Novel Unexpected Cu(II)−Thiazolidine Complex-X-ray Structure, Hirshfeld Surface Analysis, and Biological Studies. *Molecules* **2022**, *27*, 4583.

(11) Altowyan, M. S.; Soliman, S. M.; Al-Wahaib, D.; Barakat, A.; Ali, A. E.; Elbadawy, H. A. Synthesis of a New Dinuclear Ag(I) Complex with Asymmetric Azine Type Ligand: X-ray Structure and Biological Studies. *Inorganics* **2022**, *10*, 209.

(12) Barbazán, P.; Carballo, R.; Covelo, B.; Lodeiro, C.; Lima, J. C.; Vázquez-López, E. M. Synthesis, Characterization, and Photophysical Properties of 2-Hydroxybenzaldehyde [(1 E)-1-pyridin-2-ylethylidene]hydrazone and Its Rhenium(I) Complexes. *Eur. J. Inorg. Chem.* **2008**, *2008*, 2713−2720.

(13) Chile, N. E.; Haldhar, R.; Godffrey, U. K.; Chijioke, O. C.; Umezuruike, E. A.; Ifeoma, O. P.; Oke, M. O.; Ichou, H.; Arrousse, N.; Kim, S. C.; et al.etal. Theoretical Study and Adsorption Behavior of Urea on Mild Steel in Automotive Gas Oil (AGO) Medium. *Lubricants* **2022**, *10*, 157.

(14) Beda, R. H. B.; Niamien, P. M.; Bilé, A. E. B.; Trokourey, A. Inhibition of Aluminium Corrosion in 1.0 M HCl by Caffeine: Experimental and DFT Studies. *Adv. Chem.* **2017**, *2017*, 6975248.

(15) Quadri, T. W.; Olasunkanmi, L. O.; Fayemi, O. E.; Akpan, E. D.; Lee, H.; Lgaz, H.; Verma, C.; Guo, L.; Kaya, S.; Ebenso, E. E. Multilayer perceptron neural network-based QSAR models for the assessment and prediction of corrosion inhibition performances of ionic liquids. *Comput. Mater. Sci.* **2022**, *214*, 111753.

(16) Erdogan, S.; Safi, Z. S.; Kaya, S.; Isın, D. O.; Guo, L.; Kaya, C. A computational study on corrosion inhibition performances of novel quinoline derivatives against the corrosion of iron. *J. Mol. Struct.* **2017**, *1134*, 751−761.

(17) El-Mokadema, T. H.; Hashema, A. I.; Abd El-Sattar, N. E. A.; Dawooda, E. A.; Abdelshafib, N. S. Green synthesis, electrochemical, DFT studies and MD simulation of novel synthesized thiourea derivatives on carbon steel corrosion inhibition in 1.0 M HCl. *J. Mol. Struct.* **2023**, *1274*, 134567.

(18) Guo, L.; Safi, Z. S.; Kaya, S.; Shi, W.; Tüzün, B.; Altunay, N.; Kaya, C. Anticorrosive Effects of Some Thiophene Derivatives Against the Corrosion of Iron: A Computational Study. *Front. Chem.* **2018**, *6*, 155.

(19) Hsissou, R. Review on epoxy polymers and its composites as a potential anticorrosive coatings for carbon steel in 3.5% NaCl solution: Computational approaches. *J. Mol. Liq.* **2021**, *336*, 116307.

(20) Allal, H.; Belhocine, Y.; Zouaoui, E. Computational study of some thiophene derivatives as aluminum corrosion inhibitors. *J. Mol. Liq.* **2018**, *265*, 668−678.

(21) Ituen, E.; Akaranta, O.; James, A. Evaluation of Performance of Corrosion Inhibitors Using Adsorption Isotherm Models: An Overview. *Chem. Sci. Inter. J.* **2017**, *18*, 1−34.

(22) Annon, I.; Abbas, A.; Al-Azzawi, W. K.; Hanoon, M. M.; Alamiery, A. A.; Wan Isahak, W.; Kadhum, R. A. A. H. Corrosion inhibition of mild steel in a hydrochloric acid environment using thiadiazole derivative: Weight loss, thermodynamics, adsorption and computational investigations. *S. Afr. J. Chem. Eng.* **2022**, *41*, 244−252.

(23) Jasim, A. S.; Rashid, K. H.; AL-Azawi, K. F.; Khadom, A. A. Synthesis of a novel pyrazole heterocyclic derivative as corrosion inhibitor for low-carbon steel in 1M HCl: Characterization,

gravimetrical, electrochemical, mathematical, and quantum chemical investigations. *Results Eng.* **2022**, *15*, 100573.
(24) Rbaa, M.; Galai, M.; Abousalem, A. S.; Lakhrissi, B.; Ebn Touhami, M.; Warad, I.; Zarrouk, A. Synthetic, spectroscopic characterization, empirical and theoretical investigations on the corrosion inhibition characteristics of mild steel in molar hydrochloric acid by three novel 8-hydroxyquinoline derivatives. *Ionics* **2020**, *26*, 503−522.
(25) Chaouiki, A.; Chafiq, M.; Lgaz, H.; Al-Hadeethi, M. R.; Ali, I. H.; Masroor, S.; Chung, I.-M. Green Corrosion Inhibition of Mild Steel by Hydrazone Derivatives in 1.0 M HCl. *Coatings* **2020**, *10* (7), 640.
(26) Beda, R. H. B.; Niamien, P. M.; Bilé, E. B. A.; Trokourey, A. Inhibition of Aluminium Corrosion in 1.0 M HCl by Caffeine: Experimental and DFT Studies. *Adv. Chem.* **2017**, *2017*, 1−10.
(27) Ouakki, M.; Galai, M.; Benzekri, Z.; Aribou, Z.; Ech-Chihbi, E.; Guo, L.; Dahmani, K.; Nouneh, K.; Brichef, S.; Boukhris, S.; Cherkaoui, M. A detailed investigation on the corrosion inhibition effect of by newly synthesized pyran derivative on mild steel in 1.0 M HCl: Experimental, surface morphological (SEM-EDS, DRX& AFM) and computational analysis (DFT & MD simulation). *J. Mol. Liq.* **2021**, *344*, 117777.
(28) Ouattara, S.; Tigori, M. A.; Kouakou, V.; Niamien, P. M.; Trokourey, A. Inhibition Properties of Doxycycline for Copper Corrosion in 1M Nitric Acid Solution: Experimental and Quantum Chemical Studies. *J. Pharm. Chem.* **2018**, *5*, 29−44.
(29) Huang, L.; Yang, K. P.; Zhao, Q.; Li, H. J.; Wang, J. Y.; Wu, Y. C. Corrosion resistance and antibacterial activity of procyanidin B2 as a novel environment-friendly inhibitor for Q235 steel in 1 M HCl solution. *Bioelectrochemistry* **2022**, *143*, 107969.
(30) Desai, P. S.; Kapopara, S. M. Inhibitory action of xylenol orange on aluminum corrosion in hydrochloric acid solution. *Ind. J. Chem. Tech.* **2014**, *21*, 139−145.
(31) El-Sayed, A.-R.; Mohamed, A. E.; Hassan, F. S. M.; El-Mahdy, M. S. Influence of Titanium Additions to Aluminum on the Microhardness Value and Electrochemical Behavior of Synthesized Aluminum-Titanium Alloy in Solutions of HCl and H_3PO_4. *J. Mater. Eng. Perform.* **2023**, *32*, 1760−1777.
(32) Sithuba, T.; Masia, N. D.; Moema, J.; Murulana, L. C.; Masuku, G.; Bahadur, I.; Kabanda, M. M. Corrosion inhibitory potential of selected flavonoid derivatives: Electrochemical, molecular···Zn surface interactions and quantum chemical approaches. *Results Eng.* **2022**, *16*, 100694.
(33) Abdel Hameed, R. S.; Aleid, G. M. S.; Mohammad, D.; Badr, M. M.; Huwaime, B.; Suliman, M. S.; Alshammary, F.; Abdallah, M. Spinacia oleracea Extract as Green Corrosion Inhibitor for Carbon Steel in Hydrochloric Acid Solution. *J. Int. Electrochem. Sci.* **2022**, *17*, 221017.
(34) Pais, M.; Rao, P. Electrochemical and physicochemical studies for adsorption of Bovine serum albumin for corrosion mitigation of zinc. *J. Mater. Chem. Phys.* **2022**, *283*, 126034.
(35) Mobin, M.; Aslam, R.; Salim, R.; Kaya, S. An investigation on the synthesis, characterization and anti-corrosion properties of choline-based ionic liquids as novel and environmentally friendly inhibitors for mild steel corrosion in 5% HCl. *J. Colloid Interface Sci.* **2022**, *620*, 293−312.
(36) Radi, A.; Aouniti, A.; El Massoudi, M.; Radi, S.; Kaddouri, M.; Chelfi, T.; Jmiai, A.; El Asri, A.; Hammouti, B.; Warad, I.; et al.etal. Mitigation Effect Of Novel Bipyrazole Ligand And Its Copper Complex On The Corrosion Behavior Of Steel In Hcl: Combined Experimental And Computational Studies. *J. Chem. Phys. Lett.* **2022**, *795*, 139532.
(37) Giraldo, F.; Echavarría, A. M.; Bejarano, G. Corrosion performance of TiAlVN-Ag nanocomposite coating deposited by reactive direct current magnetron sputtering. *Thin Solid Films* **2022**, *761*, 139518.
(38) Ayoola, A. A.; Babalola, R.; Durodola, B. M.; Alagbe, E. E.; Agboola, O.; Adegbile, E. O. Corrosion inhibition of A36 mild steel in 0.5 M acid medium using waste citrus limonum peels. *Results Eng.* **2022**, *15*, 100490.
(39) Abdelwedoud, B. O.; Damej, M.; Tassaoui, K.; Berisha, A.; Tachallait, H.; Bougrin, K.; Mehmeti, V.; Benmessaoud, M. Inhibition effect of N-propargyl saccharin as corrosion inhibitor of C38 steel in 1M HCl, experimental and theoretical study. *J. Mol. Liq.* **2022**, *354*, 118784.
(40) Karim, W. O. Electropolishing of pure metallic nickel and cobalt in choline chloride-propylene glycol eutectic liquid: an electrochemical study using. *Electrochemistry* **2022**, *90*, 057005.
(41) Gebril, M. A.; Bedair, M. A.; Soliman, S. A.; Bakr, M. F.; Mohamed, M. B. I. Experimental and computational studies of the influence of non-ionic surfactants with coumarin moiety as corrosion inhibitors for carbon steel in 1.0 M HCl. *J. Mol. Liq.* **2022**, *349*, 118445.
(42) Galai, M.; Rbaa, M.; Serrar, H.; Ouakki, M.; Ech-Chebab, A.; Abousalem, A. S.; Ech-Chihbi, E.; Dahmani, K.; Boukhris, S.; Zarrouk, A.; et al.etal. S-Thiazine as effective inhibitor of mild steel corrosion in HCl solution: Synthesis, experimental, theoretical and surface assessment. *Colloids Surf., A* **2021**, *613*, 126127.
(43) Alaoui, K.; Ouakki, M.; Abousalem, A. S.; Serrar, H.; Galai, M.; Derbali, S.; Nouneh, K.; Boukhris, S.; Ebn Touhami, M.; El Kacimi, Y. Molecular dynamics, Monte-Carlo simulations and atomic force microscopy to study the interfacial adsorption behaviour of some *Triazepine Carboxylate* compounds as corrosion inhibitors in acid medium. *J. Bio Tribo Corros.* **2019**, *5* (1), 1−16.
(44) Ech-Chebab, A.; Dahmani, K.; Hsissou, R.; El Khouja, O.; Verma, D. K.; Berdimurodov, E.; Erdoğan, Ş.; Tüzün, B.; Lachhab, R.; Ejbouh, A.; Galai, M. Anticorrosion properties of the epoxy polymer TGETBAU for mild steel in a solution of HCl (1.0 M): Experimental and computational approaches. *J. Mol. Struct.* **2023**, *1284*, 135441.
(45) Chile, N.; Haldhar, R.; Godffrey, U. K.; Chijioke, O. C.; Umezuruike, E. A.; Ifeoma, O. P.; Oke, M. O.; Ichou, H.; Arrousse, N.; Kim, S.-C.; Dagdag, O.; Ebens, E. E.; Taleb, M. Theoretical Study and Adsorption Behavior of Urea on Mild Steel in Automotive Gas Oil (AGO) Medium. *Lubricants* **2022**, *10* (7), 157.
(46) El-Azabawya, O. E.; Higazya, S. A.; Al-Sabagha, A. M.; Abdel-Rahmanb, A. A. H.; Nasser, N. M.; Khamis, E. A. Studying the temperature influence on carbon steel in sour petroleum media using facilely-designed Schiff base polymers as corrosion inhibitors. *J. Mol. Struct.* **2023**, *1275*, 134518.
(47) Ebenso, E. E.; Arslan, T.; Kandemirl, F.; Love, I.; Ögretir, C.; Saracoğlu, M.; Umoren, S. A. Theoretical Studies of Some Sulphonamides as Corrosion Inhibitors for Mild Steel in Acidic Medium. *Int. J. Quantum Chem.* **2010**, *110*, 2614−2636.
(48) Elaryian, H. M.; Bedair, M. A.; Bedair, A. H.; Aboushahbad, R. M.; Fouda, A. E. S. Corrosion mitigation for steel in acid environment using novel p-phenylenediamine and benzidine coumarin derivatives: synthesis, electrochemical, computational and SRB biological resistivity. *RSC Adv.* **2022**, *12*, 29350−29374.
(49) Oyeneyin, O.; Akerele, D.; Ojo, N.; Oderinlo, O. Corrosion Inhibitive Potentials of some 2H-1-benzopyran2-one Derivatives-DFT Calculations. *J. Bionterface. Res.* **2021**, *11*, 13968−13981.
(50) Gázquez, J. L.; Cedillo, A.; Vela, A. Electrodonating and Electroaccepting Powers. *Phys. Chem.* **2007**, *10*, 1966−1970.
(51) Chattaraj, P. K.; Sarkar, U.; Roy, D. R. *Electrophilicity Index* **2006**, *106*, 2065−2091.
(52) Salinas-Solano, G.; Porcayo-Calderon, J.; Escalera, L. M. M.; Canto, J.; Casales-Diaz, M.; Sotelo-Mazon, O.; Henao, J.; Martinez-Gomez, L. Development and evaluation of a green corrosion inhibitor based on rice bran oil obtained from agro-industrial waste, Ind. *Ind. Crops Prod.* **2018**, *119*, 111−124.
(53) Iorhuna, F.; Muhammad, A. S.; Muham, A. Quinazoline Derivatives as Corrosion Inhibitors on Aluminium Metal Surface: A Theoretical Study. *Adv. J. Chem., Sec. A* **2023**, *6*, 71−84.
(54) Moussa, M. N. H.; El-Far, A. A.; El-Shafei, A. A. The use of water-soluble hydrazones as inhibitors for the corrosion of C-steel in acidic medium. *Mater. Chem. Phys.* **2007**, *105*, 105−113.

https://doi.org/10.1021/acsomega.4c00199
ACS Omega 2024, 9, 16469−16485